Applied Geochemistry 159 (2023) 105843

Contents lists available at ScienceDirect

Applied Geochemistry

journal homepage: www.elsevier.com/locate/apgeochem

Diffusion of HTO, ^{36}Cl and ^{22}Na in the Mesozoic rocks of northern Switzerland: I. Effective diffusion coefficients and capacity factors across the heterogeneous sediment sequences

Luc R. Van Loon [a,*], Petar Bunic [a], Sabrina Frick [b], Martin A. Glaus [a], Raphael A.J. Wüst [c,d]

[a] Paul Scherrer Institut, Forschungsstrasse 111, 5232, Villigen PSI, Switzerland
[b] Departement Bau, Verkehr und Umwelt, Entfelderstrasse 22, 5001, Aarau, Switzerland
[c] Nagra, Hardstrasse 73, 5430, Wettingen, Switzerland
[d] Earth and Environmental Science, James Cook University, 4811, Townsville, Australia

ARTICLE INFO

Editorial handling by: Adrian Bath

Keywords:
Geometrical factor
Mineralogy
Diffusion correlations
Opalinus Clay
Heterogenous sediments

ABSTRACT

Argillaceous rocks are currently being examined worldwide as potential host rocks for repositories for radioactive waste and spent fuel due to their favourable characteristics such as the self-sealing ability or limited diffusive transport of fluids, solutes or gases. In this study, through-diffusion experiments focused on rock samples with different mineralogical compositions taken from deep boreholes in the Mesozoic rock sequence of northern Switzerland, to determine diffusion parameters of HTO, $^{36}Cl^-$ and $^{22}Na^+$ perpendicular to the bedding plane. Both effective diffusion coefficients and accessible porosities were calculated from the data obtained. In the Opalinus Clay, the primary selected host rock of the repository, the effective diffusion coefficients (D_e) and accessible porosity values (ε) of the neutral species HTO within and across all study areas are relatively consistent ($D_e = 8.8 \pm 1.9 \times 10^{-12}$ m^2 s^{-1}; $\varepsilon = 0.12 \pm 0.02$), indicating that the material can be considered homogeneous in terms of diffusion properties. Importantly, the chemical composition of the pore water has no effect on the values of the effective diffusion coefficients of HTO. On the other hand, the rocks above and below the Opalinus Clay, up to the next aquifer, consist of tight sedimentary units (carbonates, siliciclastics including argillaceous rocks) with a wider range of diffusion coefficients, indicating a higher level of heterogeneity. The diffusion coefficients of anions, such as $^{36}Cl^-$, tend to be smaller due to anion exclusion effects, while those of cations, such as $^{22}Na^+$, tend to be larger due to surface enhanced diffusion. The extent of these effects is largely determined by the composition of the pore water, and – in the case of cations – by the extent of sorption which depends also on the sorption capacity – indicated by the cation exchange capacity - of the solid. As a result, variations in the effective diffusion coefficient of $^{36}Cl^-$ and $^{22}Na^+$ can be observed firstly between different rock types (i.e. composition, fabric), and secondly between the different study areas due to differences in the chemical composition of the pore waters in contact with the solid phase.

Based on the analysis of around 130 samples, it has been observed that the diffusion coefficients of the Mesozoic units in northern Switzerland exhibit a significant correlation with the total clay content of the rocks. These findings pave the way for the establishment of a diffusion database for the relevant elements under consideration in the Swiss radioactive waste programme and the Safety Case.

1. Introduction

A comprehensive exploratory program examining the Mesozoic sedimentary sequence of northern Switzerland investigated several (9) deep boreholes (Mazurek et al., 2023) with core recoveries to characterize the geological and hydrogeological properties for the future deep geological disposal of various types of radioactive waste (Nagra, 2021). The geological sequence from the Mesozoic era in Switzerland can be divided into three schematic units, with the Opalinus Clay forming the core unit and the host rock for the potential waste repository. The Jurassic-age Opalinus Clay (OPA) is a clay-rich rock unit that is over 100 m thick. The second sedimentary package overlays the Opalinus Clay

* Corresponding author.
E-mail address: luc.vanloon@psi.ch (L.R. Van Loon).

https://doi.org/10.1016/j.apgeochem.2023.105843
Received 14 March 2023; Received in revised form 15 August 2023; Accepted 8 November 2023
Available online 22 November 2023

and consists of Dogger and Malm tight clay-, carbonate-, and silt-/-sandstone rocks that extend up to the next aquifer in the Malm. The third sequence occurs below the Opalinus Clay and is composed of Lias and Keuper/Triassic aged sediments of mostly tight clay-, carbonate-, anhydrite, and silt-/sandstone rocks down to the next aquifer (either in the Keuper or the Triassic Muschelkalk, see Mazurek et al., 2023). Both over- and underlying units have a high proportion of clay-rich rocks, and the subunits with variable rock types also vary in thickness. Further information about thickness and composition variability can be found in Mazurek et al. (2023).

Claystones have been one of the potential rock types of the Swiss radioactive waste programme since the late 1980ties (Nagra, 2002), with a focus on the Jurassic-age Opalinus Clay. The Paul Scherrer Institute has played a leading role in investigating diffusion in the Opalinus Clay, with studies conducted on samples from the Mont Terri Underground Rock Laboratory (MT-URL) located in the northwestern part of Switzerland (Bossart and Thury, 2007) and the deep boreholes of Benken in the Zürich Nordost area (Van Loon and Soler, 2003) and Schlattingen (Wersin et al., 2013) (Fig. 1). Despite the limited number of samples, the studies obtained reliable results of the effective diffusion coefficients (D_e) and accessible porosities (ε) for neutral species (HTO), that were confirmed by other studies on MT-URL samples (Wu et al., 2009; Joseph et al., 2013; Kaplan, 2013; Lübke, 2015). In addition, the laboratory diffusion studies clearly demonstrated the existence of anion exclusion in Opalinus Clay (Van Loon et al., 2003). This phenomenon, due to anions being repelled from the negatively charged surface of clay minerals, was first described by Dutt and Low (1962) in clay-rich soils, and was subsequently applied in various other studies (Bazer-Bachi et al., 2006; Descostes et al., 2008; Aertsens et al., 2008; Cavé et al., 2009). A comprehensive discussion and newly developed approaches based on the introduction of interlayer equivalent pores, a Donnan pore space and uncharged pores was later presented by Wigger and Van Loon (2017). Further progress and details of the anion exclusion effect and new evidence for differences in exclusion of anions in argillaceous rocks from the new borehole campaign is now also documented by Zwahlen et al. (2023).

During the early studies of diffusion properties of the Opalinus Clay, measurements using $^{22}Na^{+}$, $^{85}Sr^{2+}$ and $^{134}Cs^{+}$ provided evidence of surface-enhanced diffusion (Appelo et al., 2010). This effect could be successfully modelled using a multispecies transport model implemented in PHREEQC that also incorporated a Donnan approach to account for anion exclusion and surface diffusion (Appelo and Wersin, 2007). This model was subsequently expanded to include surface diffusion of transition metals (Glaus et al., 2015) and lanthanides (Glaus et al., 2020), as well as competitive effects of charged species in diffusion (Glaus et al., 2021). Another significant milestone was achieved during the early phase of working with Opalinus Clay when it was demonstrated that sorption in compacted systems (Opalinus Clay) is comparable to sorption on loose (crushed) material (Van Loon et al., 2009).

The early work also investigated temperature and anisotropy effects on the diffusion behaviour. Temperature-dependent diffusion tests with HTO, $^{36}Cl^{-}$ and $^{22}Na^{+}$ revealed that the temperature effect on diffusion can be appropriately described by the Arrhenius equation within a temperature range between 5 and 70 °C (Van Loon et al., 2005) using an activation energy of approximately 20 ± 2 kJ mol^{-1}. Savoye et al. (2011) came to the same conclusions for diffusion of HTO, $^{36}Cl^{-}$ and $^{22}Na^{+}$ in Callovo-Oxfordian argillite, but not for diffusion of $^{137}Cs^{+}$, for which the activation energy was only 9 kJ mol^{-1}. Since shales and clay-rich rocks are characterised by clay platelets with a preferred horizontal orientation, anisotropic hydraulic and mechanical properties are expected. Van Loon et al. (2004) conducted diffusion measurements in both parallel (par) and perpendicular (per) orientation to the bedding plane of the Opalinus Clay. The results revealed diffusion anisotropy factors, $F_{an} = D_{e,par}$: $D_{e,per}$, ranging from 4 (Mont Terri) to 6 (Benken). A follow-up field experiment conducted in Mont Terri found that the in situ anisotropy ratios for diffusion were larger for HTO and Na-22 (~5) than for anions (~3–4 for Br and I) (Gimmi et al., 2014). These results provide evidence of the presence of diffusion anisotropy, which is expected given the layered structure of these clay-rich rocks of the Opalinus Clay (Wenk et al., 2008). Similar conclusions were made by Xiang et al. (2013) for Ordovician sedimentary rocks from the Michigan Basin in southwest Ontario (Canada). It could also be demonstrated that confining pressure had a small effect on the effective diffusion coefficient, but no measurable effect on the accessible porosity (Van Loon and

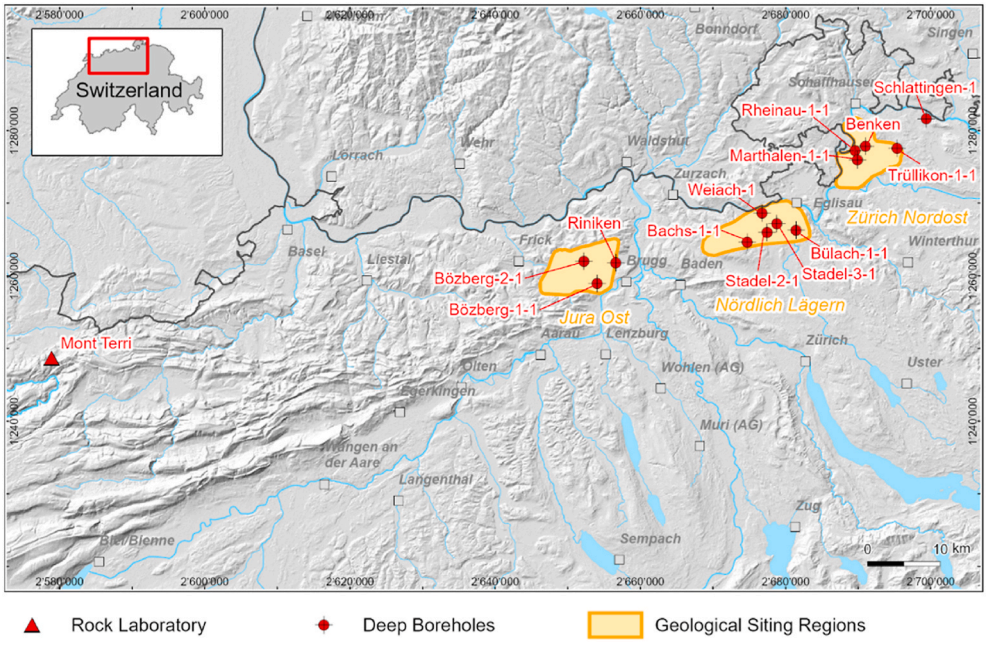

Fig. 1. Cartographic representation illustrating the geographical region of northern Switzerland, inclusive of the three study areas, namely Jura Ost, Nördlich Lägern, and Zürich Nordost. The map features the borehole sites referred to in this study, as well as the location of the Mont Terri Underground rock laboratory, which is under the guidance of Swisstopo. Mont Terri URL (since 1995), Benken (Nagra, 2021), and Schlattingen (Wersin et al., 2013) provided Opalinus Clay samples for previous diffusion experiments.

Soler, 2003; Xiang et al., 2016).

For stage 2 of the SGT (Swiss Sectoral Plan of Deep Geological Repositories) only a few Opalinus Clay samples from borehole Schlattingen (close to the Zürich Nordost study area) (Fig. 1) have been evaluated for effective diffusion coefficients of HTO, $^{36}Cl^-$ and $^{22}Na^+$ (Van Loon, 2014), with values in good agreement with those from the Opalinus Clay of the Mont Terri URL and the Benken borehole (Van Loon et al., 2004) (see Fig. 1 for locations). In addition to laboratory diffusion work on cm-scale samples, several field diffusion studies in the Opalinus Clay have been performed in the Mont Terri URL on a large scale of several decimetres (Leupin et al., 2017 and references therein). The results of these field studies demonstrate excellent agreement with laboratory measurements. Such field-to laboratory-scale comparisons increase confidence in the reliability of the early laboratory work. Also, extensive studies on natural tracer profiles showed that diffusion is the dominant transport process over several million years (Mazurek et al., 2011).

The main objective of previous diffusion studies was to obtain initial insights and understanding of diffusion processes in the Opalinus Clay, and to utilize this knowledge to develop a diffusion database (DDB) that can be applied in long-term safety assessment studies. The first DDB (Van Loon, 2014) was created using Archie's relationship, which linked effective diffusion coefficients to accessible porosity. Van Loon and Mibus (2015) developed an extended version of Archie's law (e-Archie) primarily based on literature data from different sedimentary rocks. However, only a limited amount of data covered the Opalinus Clay and even less data was derived from the adjacent over- or underlying units for the development of the e-Archie approach.

More recent studies have shown that molecular diffusion is also the main transport mechanism for radionuclides in clay-rich layers adjacent to the Opalinus Clay (Van Loon, 2014; Gimmi and Waber, 2004; Wersin et al., 2018). In 2018, Nagra started a new exploration programme aimed at acquiring an extensive and comprehensive dataset on diffusion, encompassing the Opalinus Clay and the sedimentary packages above and below it, up to the subsequent aquifers in all three study areas (Fig. 1 and Mazurek et al., 2023). This initiative constituted a primary objective, alongside the imperative for a new diffusion database. Previous studies have suggested that the Opalinus Clay may have a uniform diffusion behaviour. However, the layers above it, such as the Dogger and Malm sequence, and the layers located below it, such as the Lias, Keuper/Triassic sequence, show considerable heterogeneity (see Mazurek et al., 2023).

The main objective of this study is to measure the diffusion properties of HTO, $^{36}Cl^-$ and $^{22}Na^+$ in samples from all the different rock types across the lithostratigraphic profile of interest (Opalinus Clay and sedimentary units that occur between the overlying Malm and underlying Keuper or Triassic aquifers). This approach allows us to assess the spatial distribution of diffusion properties across different geological units and to determine the degree of heterogeneity of diffusion properties. Additionally, another aim of the study is to identify any correlations between diffusion parameters and material properties, such as mineral composition or microfabric. These correlations can provide valuable information for understanding transport of dissolved species through heterogeneous sedimentary sequences (Bollermann et al., 2022).

The diffusion properties are basically expressed as the effective diffusion coefficients and capacity factors. The capacity factors are subsequently interpreted in terms of accessible porosity in the case of HTO and $^{36}Cl^-$ and in terms of sorption distribution ratios in the case of $^{22}Na^+$. This contribution is the first part of three related contributions in this Special Issue and provides the basic set of diffusion data for all tracers and the technical information related to the measurements. It presents the results of the effective diffusion coefficients for all tracers but focuses mainly on the interpretation in terms of the effective diffusion coefficients of HTO, which is treated as an inert reference tracer and for which all measurements can be summarised in a single population. The results of the charged tracers ($^{36}Cl^-$ and $^{22}Na^+$) cannot be explained quantitatively in the same context because their diffusion properties depend on the surface properties of the charged clay minerals and the composition of the pore waters used for the experiments. For this reason, the interpretation of those data is provided in a second part of this Special Issue (Glaus et al., 2023). The third part, a companion paper by Van Laer et al. (2023), finally presents a benchmark study of diffusion measurement and modelling approaches carried out at PSI (Switzerland) and at SCK-CEN (Belgium) using a selection of five rock samples from the entire series of diffusion samples investigated: four Opalinus Clay samples and one clayrich sample from the underlying Staffelegg Formation.

2. Materials and methods

2.1. Rock samples and sample preparation

Sample material was collected from seven deep boreholes drilled in the three study areas, Jura Ost (JO), Nördlich Lägern (NL), and Zürich Nordost (ZNO) in the northern part of Switzerland (see Fig. 1 and also Mazurek et al., 2023). There, the core material was derived from Bözberg1-1 (BOZ1-1) and Bözberg2-1 (BOZ2-1), located in JO; Bülach1-1 (BUL1-1), Stadel2-1 (STA2-1) and Stadel3-1 (STA3-1), all three located in NL; Trüllikon1-1 (TRU1-1) and Marthalen1-1 (MAR1-1), both located in ZNO. Details of the locations are provided elsewhere (Mazurek et al., 2023). In the case of BOZ1-1, BUL1-1 and TRU1-1, samples of Opalinus Clay (OPA), and samples from the overlying Dogger and Malm and the underlying Lias, Keuper and Triassic sediments, were studied. In the case of BOZ2-1, STA2-1, STA3-1 and MAR1-1 only samples of the overlying and underlying sedimentary sequences were used. A comprehensive overview of all samples can be found in Tables S1–S3 in the supporting information.

Furthermore, this investigation builds upon previous studies and findings from isotopic diffusion research conducted as part of prior exploration initiatives. In 1995, the attention of establishing a deep geological repository for radioactive spent fuel and waste in Switzerland transitioned towards the Opalinus Clay, leading to the planning and execution of an exploratory borehole in Benken (1998–1999), situated west of Winterthur (Fig. 1), that penetrated the subsurface to a depth of 1007 m below the surface (Nagra, 2001). In 2012, Schlattingen-1 was another exploratory borehole (geothermal energy) which provided sample material for diffusion testing of the Opalinus Clay (Wersin et al., 2013).

The samples used in the diffusion experiments for this study were selected from the new exploratory boreholes and prepared at the Institute of Geological Sciences, University of Bern. From each sealed 200 mm long rock sample, a 55 mm long cylinder with a diameter of 64 mm was sub-cored after initial CT scan analysis that helped to identify homogeneous rock portions (Fig. 2). The remainder of the material was used for auxiliary investigations, including the quantification of porosity, mineralogy and microfabric and the sample material was sealed immediately after the preparatory step. The cylinder was drilled perpendicular to the bedding plane by wet (tap water) drilling using a Hilti® drilling machine. This subcore was embedded in epoxy resin (Epofix, Struers, Germany). After hardening at 40 °C overnight, the sample was cut dry into one or two slices with a thickness of 10–14 mm (Fig. 2). Atmospheric oxic condition exposure of the samples was limited during sample preparation and material not used was resealed immediately, while material being prepared was sealed following the preparatory steps.

2.2. Synthetic porewaters (SPW)

The experimental porewater compositions utilized in this study were derived from preliminary data obtained through advective displacement laboratory analyses of samples sourced from the corresponding boreholes situated within the study regions (BUL1-1: Mazurek et al., 2021;

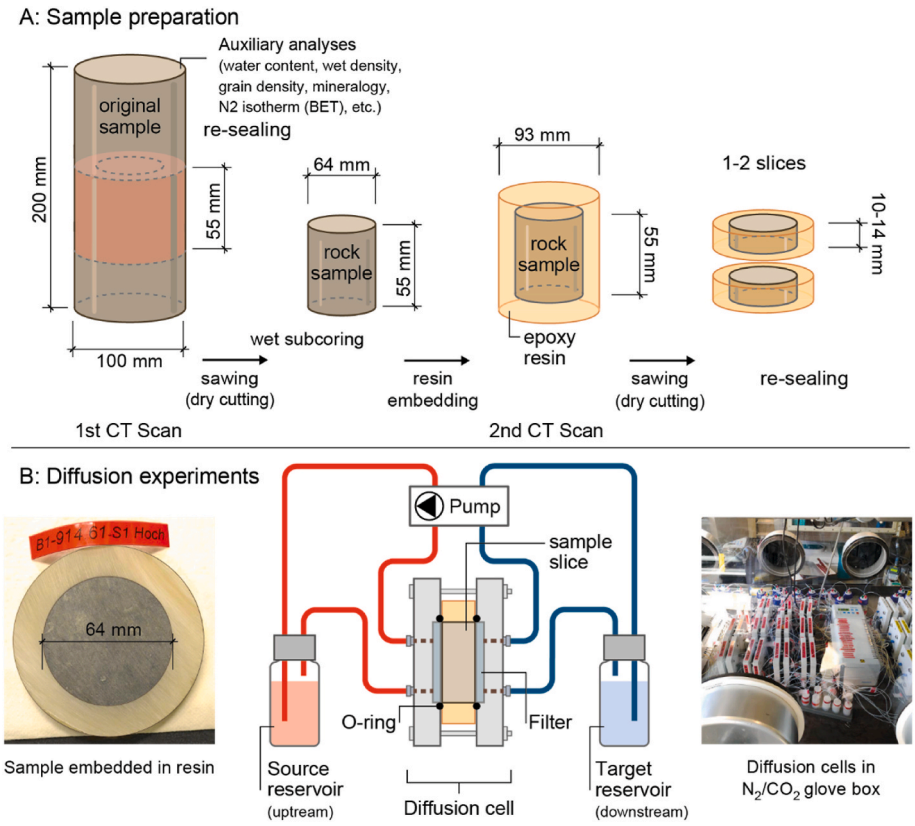

Fig. 2. A: Schematic representation of the sample preparation procedure employed by the University of Bern. B: The diffusion set-up scheme is depicted in the middle, with accompanying images of the embedded sample (left) and diffusion cells in the glove box (right).

TRU1-1: Aschwanden et al., 2021; BOZ1-1: Wersin et al., 2022). The concentrations of initial aliquots were modified via geochemical equilibrium modelling to relevant mineral equilibria and an atmospheric pCO_2, using chemical equilibration calculations in PHREEQC based on the PSI-Nagra Thermodynamic Database (Hummel and Thoenen, 2023). A distinct composition was established for each study area to account for regional variability, as presented in Table 1. While this approach does not account for vertical variability across the sedimentary units within a borehole, this procedure is defendable because the misfit remains limited, and the effect of the porewater composition on the diffusion parameters within a borehole is negligible (HTO) or relatively insignificant ($^{36}Cl^-$ and $^{22}Na^+$).

Table 1
Composition of the synthetic porewaters (SPW) used in the diffusion measurements.

Element	Concentration (M)			
	BOZ1-1/BOZ2-1	BUL1-1	STA2-1/STA3-1	TRU1-1/MAR1-1
Na	1.40×10^{-1}	3.43×10^{-1}	1.56×10^{-1}	2.44×10^{-1}
K	7.76×10^{-4}	1.91×10^{-3}	1.91×10^{-3}	1.64×10^{-3}
Ca	9.24×10^{-3}	3.83×10^{-2}	3.50×10^{-2}	2.22×10^{-2}
Mg	3.94×10^{-3}	1.76×10^{-2}	1.76×10^{-2}	1.56×10^{-2}
Sr	1.15×10^{-4}	3.33×10^{-4}	3.33×10^{-4}	2.89×10^{-4}
Cl	8.28×10^{-2}	4.02×10^{-1}	2.19×10^{-1}	2.72×10^{-1}
S (as SO_4)	4.21×10^{-2}	2.75×10^{-2}	2.22×10^{-2}	2.43×10^{-2}
C (as HCO_3)	7.05×10^{-4}	4.13×10^{-4}	4.13×10^{-4}	4.87×10^{-4}
pH	7.90	7.56	7.56	7.68
[a]I	0.190	0.505	0.306	0.354

[a] As calculated from speciation calculations with PHREEQC.

MAR1-1, TRU1-1 and BUL1-1 were the first set of boreholes and the identified PW composition of TRU1-1 and MAR1-1 was identical in contrast to BUL1-1 with a markedly elevated salt concentration (~13′000 mg/l Cl). Although BUL1-1- lies within the NL study area, the porewaters of both STA2-1 and STA3-1 were more closely aligned with the one of TRU1-1 and MAR1-1, which all were modified to 8000 mg/l Cl and slightly lower Ca and SO_4 concentrations. The western study area, with boreholes BOZ1-1 and BOZ2-1, contained the lowest salinity porewater composition (~2000 mg/l Cl). The synthetic pore waters (SPW) were prepared by dissolving Ca-, Mg-, Na- and K-salts in ultrapure water. The water was degassed by boiling and purging nitrogen (N_2) through it for the duration of 2 h prior to usage. Subsequently, the heated water was then transferred to a N_2-regulated glovebox that had an O_2 content <0.1 ppm and $CO_2 = 400 \pm 10$ ppm, where it was allowed to cool and equilibrate with the glovebox atmosphere for two days. The CO_2 level in the glovebox was identical to the atmospheric CO_2 level because all porewater calculations were done at atmospheric CO_2 level (see section 2.2). After this time, specific quantities of salt were dissolved in the predetermined volume of water (slightly less than the final volume). After one day, the pH of the solution was adjusted to the target value by adding small amounts of a 1 M NaOH solution, and water was added to achieve the desired volume.

2.3. Diffusion

A detailed description of the diffusion set-up is provided in Van Loon (2014) with a scheme presented in Fig. 2. The prepared diffusion samples were positioned between two porous stainless-steel filters

(thickness 1.2 mm; diameter 65 mm; porosity 0.4) and fixed within the diffusion cells, with the bedding plane perpendicular to the direction of diffusion. The use of end plates and porous filters provides a rigid confinement for the clay sample limiting the possibility of swelling and potential disintegration of the samples. The use of the porous filters provides a homogeneous contact of the fluid and the clay surface ensuring thus a homogeneous concentration boundary condition for diffusion. The end plates were secured by a set of four bolts, without the control of confining pressure. Previous studies have revealed that confining pressure has a minimal, insignificant effect on diffusion (Van Loon and Soler, 2003; Xiang et al., 2016). The cells were connected to two reservoirs, namely a 100 ml glass flask and a 20 ml polyethylene β-vial, both containing 20 ml of synthetic pore water that was circulated using a peristaltic pump (IPC, Ismatec, Idex corporation, USA). In the first stage, the samples were resaturated with the borehole specific synthetic porewaters (Table 1) for a period of ca. 4–5 weeks. The solutions were exchanged once per week and analysed for main anions and cations by ion chromatography (for more details see Van Loon et al., 2023). The resaturation process continued until the composition of the porewater in both source (upstream) and target (downstream) reservoirs did no longer change significantly.

In the second stage, the diffusion experiments were initiated by filling the source reservoir (100 ml glass flask) with 100 ml SPW spiked with HTO and $^{36}Cl^{-}$. The activity in this reservoir was about 500 Bq ml^{-1} for ^{3}H (ca. 4.5×10^{-10} mol dm^{-3}) and 500 Bq ml^{-1} for $^{36}Cl^{-}$ (ca. 1×10^{-5} mol dm^{-3}). The target reservoir (20 ml polyethylene β-vial) was filled with 10 ml SPW. The solution at the low concentration side (target reservoir) was regularly replaced after a time interval, Δt, of typically 2–3 days in order to keep the concentration of the tracer in this compartment as low as possible, and the radiotracers in the exchanged solution of the target reservoir analysed. The solution of the source reservoir was sampled once a week (100 μl) to analyse the radiotracers. The sampled volume was not replaced because the volume decrease due to sampling was taken into account in the modelling of the data. HTO and $^{36}Cl^{-}$ were measured with β/β discrimination by liquid scintillation counting (LSC). A detailed description of the β/β discrimination is given in Glaus et al. (2017). There, 10 ml of solution was mixed with 10 ml of Ultimagold AB in a 20 ml polyethylene β-vial and then measured with a Tricarb 2250 CA (Canberra-Packard) LSC instrument. All saturation steps and diffusion measurements were performed in an inert gas glove box under anoxic conditions ($O_2 < 0.1$ ppm; $CO_2 = 400 \pm 10$ ppm). The purpose of the presence of CO_2 in the glove box atmosphere was to prevent losses of CO_2 from the solutions and pH drifts induced thereby. The temperature in the glove box was 26.7 ± 0.8 °C.

In a third stage, the experiments with $^{22}Na^{+}$ were started as soon as the diffusion of $^{36}Cl^{-}$ and HTO had reached the steady state phase indicated by a constant flux of the tracers over time. A given amount of $^{22}Na^{+}$ tracer, resulting in an activity of about 500 Bq ml^{-1} (ca. 9.5×10^{-11} mol dm^{-3}) was added to the same source reservoir. The target side was connected to a 20 ml polyethylene β-vial (target reservoir) containing 10 ml SPW. The experimental protocol was identical to the one described for HTO/$^{36}Cl^{-}$. The $^{22}Na^{+}$ activity in the sampled solutions and source reservoir was measured by γ-counting, in which no interference with the previously measured HTO and $^{36}Cl^{-}$ occurred. A 5 ml sample of the target solution was placed in a counting vial and the activity measured in a Minaxi-γ, Autogamma 5000 series (Canberra-Packard) γ-counter. For the activity in the source reservoir, 100 μl solution was sampled and 5 ml of SPW was added to achieve the same counting geometry.

Uncertainty estimations on the values of the flux and total diffused mass are based on the uncertainty of the parameters involved to calculate these values. The procedure to estimate uncertainties is described in detail in Van Loon and Soler (2003).

2.4. Parameter estimation

Modelling of the diffusion data was done with Comsol Multiphysics® using the 'Transport of Diluted Species in Porous Media' interface involving a 1D-linear geometry for representing the filter and clay domains (Glaus et al., 2017). The concentration change in the source solution reservoir is reflected in variable boundary conditions at the interfaces between filters and solution while a zero-concentration boundary condition was applied for the target side. The calculation of the variable source boundary concentration involves the difference between the total mass present at time zero and the mass diffused from the source domain as a function of time. Best-fit parameter values and the respective parameter uncertainties (95% confidence level) were obtained from a parameter optimisation routine (using the lsqnonlin function in Matlab®), in which the Comsol Multiphysics® model is used as a Matlab® script. Glaus et al. (2017) provided a comprehensive description of the methodology, with additional information below. To fit the parameters, the cumulated diffused mass at the target side and the source concentration of the diffusing species as a function of time are utilized as the source data. The use of the average target flux data, instead of accumulated mass, yielded similar results with discrepancies that typically fall within the fitting uncertainties. Both the cumulative mass and the average target flux are derived from the measured activity which accumulated in the target reservoir solution between sample exchanges. In that sense, those quantities contain the same basic information, and only negligible numerical differences between the evaluation methods related to these quantities would be expected. In reality, the average target flux data inherently comprise systematic errors owing to inadequacies related to averaging sampling times. The comparison between the two evaluation methods (cumulative mass versus average target flux) demonstrates that the sampling regime applied is adequate for keeping the errors introduced at an acceptable level.

The adjustable parameters for all three nuclides include the effective diffusion coefficient in the clay rock and the initial concentration at time zero. Generally speaking, the capacity factor (α, [–]) was used as a third adjustable parameter. It can be written as

$$\alpha = \varepsilon \pm \rho_{br} R_d \quad (1)$$

ε is the diffusion accessible porosity, ρ_{br} the bulk-dry density (kg m^{-3}) and R_d the (sorption) distribution factor (m^3 kg^{-1}) defined as

$$R_d = \frac{C_{sorbed}}{C_{solution}} \quad (2$$

Where C_{sorbed} represents the number of species sorbed on the solid phase (mol kg^{-1}) and $C_{solution}$ is the species concentration in solution (mol m^{-3}) in equilibrium with the sorbed amount.

HTO and $^{36}Cl^{-}$ are treated as non-sorbing species ($R_d = 0$). Thereby eq. (1) reduces to $\alpha = \varepsilon$, where ε is assumed to represent the total porosity (ε_{tot}) in the case of HTO and the anion-accessible porosity (ε_{an}) in the case of $^{36}Cl^{-}$. For technical reasons, ρ_{br} is treated as the adjustable parameter instead of α in the case of HTO. ρ_{br} was related via a generic (formal) material (or grain) density (ρ_{gr}) of 2800 kg m^{-3} to the total porosity (ε_{tot}) according to the relationship:

$$\varepsilon_{tot} = 1 - \frac{\rho_{br}}{\rho_{gr}} \quad (3)$$

For this reason, the best-fit parameter value of ρ_{br} depends on the choice of ρ_g and cannot be directly compared with the sample specific data presented in Mazurek et al. (2023). However, the difference between the measured ρ_{br} using pycnometry and the optimised value in this work was at most 12%.

In the case of the $^{36}Cl^{-}$ data, the anion porosity fraction (f_{an})

$$f_{an} = \frac{\varepsilon_{an}}{\varepsilon_{tot}} \quad (4)$$

is used as the third adjustable parameter in combination with the given total porosity for HTO from the parent experiment. Similarly, R_d is used as the third adjustable parameter in the case of the $^{22}Na^+$ data via the definition of a 1-site Langmuir isotherm in which the affinity constant is chosen in a way to keep the experimental data in a 'linear sorption range' (Glaus et al., 2020). The diffusion accessible porosity of $^{22}Na^+$ is assumed to be equal the diffusion accessible porosity of HTO. For this reason, the total porosity value is selected based on the best-fit parameter value obtained from the HTO data.

While the initial concentration is an experimentally determined value, it is treated as an adjustable parameter (within a rather narrow range of possible values) if there is a discrepancy between the measured value at time zero and the extrapolation from the subsequent measurements at the following time points.

To estimate the uncertainties of the diffusion properties of the confining filters on the best-fit parameter values of the adjustable parameters, a sensitivity analysis was conducted, because there were no pertinent values determined for the diffusivity in the filters.

As the effect of the confining filters on the evaluation of the diffusion properties of the clay rock samples are rather small in these experiments, experience values from other filters (Glaus et al., 2008; Aldaba et al., 2014) were chosen. The uncertainty ranges for the experience values were chosen rather large in order to cover the potential variability among different production batches (Glaus et al., 2008). For HTO, the uncertainty bounds were 5×10^{-11} m^2 s^{-1} < D_{e_fil} < 1.5×10^{-10} m^2 s^{-1} with a preferred value of 1.0×10^{-10} m^2 s^{-1}. These upper and lower limits are used for two "bounding" parameter optimisation scenarios (in Matlab), which then generate upper and lower bounds for the adjustable parameter values (with regard to filter uncertainties). The best-fit parameter values for the preferred filter value are then calculated by averaging each of the two bounding "filter scenarios". The maximum and minimum uncertainty values obtained in the two scenarios are used as the upper and lower bounds of the best-fit parameter values. This approach is quite pragmatic to account for the effect of uncertainties of the diffusion properties of the filters on the diffusion parameters of the clay. For $^{22}Na^+$, the preferred effective diffusion coefficient for the filters is 6×10^{-11} m^2 s^{-1}, with 3×10^{-11} m^2 s^{-1} and 9×10^{-11} m^2 s^{-1} as the lower and upper, respectively, bounding values. In the case of $^{36}Cl^-$, the chosen effective diffusion coefficient for the filters is 1×10^{-10} m^2 s^{-1}. As a result of the very low effective diffusivities of this tracer in the clay, no sensitivity analysis was carried out for the filter diffusivities for this tracer.

It should be noted that the diameter of the confining filters in the experiments is slightly larger (65 ± 0.5 mm) than the diameter of the sample (63.6 ± 0.1) mm. However, a 2-D simulation (not shown) was conducted which demonstrated that the overlapping domains of the filters did not have a significant influence on the best-fit parameter values and their uncertainties.

3. Results

This study focused on the examination of Mesozoic sedimentary sequence of northern Switzerland and accessed a large number of core samples (~130) with associated geological data to comprehensively investigate the effect of sediment composition on diffusion parameters. The findings indicate that the diffusion parameters are significantly impacted by the mineralogical composition and rock parameters.

Specifically, the study focused on evaluating the effective diffusion coefficients (D_e) for HTO, $^{36}Cl^-$ and $^{22}Na^+$, the corresponding accessible porosities (ε, ε_{an}) and, in the case of $^{22}Na^+$, the distribution coefficients (R_d). The complete set of the results for all tracers, the D_e values and the quantities related to the capacity factors (accessible porosities, distribution factors) are available in Tables S1–S3 in the supplementary information. Graphical illustrations focus in the present contribution on the statistical behaviour of the D_e values of HTO and on the discussion of the various parameter dependencies observed. For the graphical representation of the parameter values related to the capacity factors, the reader is referred to the second part (Glaus et al., 2023) of the three-part contribution to the Special Issue.

Additionally, the effective diffusion coefficients for HTO, $^{36}Cl^-$ and $^{22}Na^+$ are plotted against the depth for each study area (Fig. 3). For each individual study area (Fig. 1), data from each borehole were projected onto the area's reference borehole, which were BOZ1-1 for Jura Ost, STA2-1 for Nördlich Lägern, and TRU1-1 for Zürich Nordost. This approach was adopted because in some boreholes, diffusion analysis focused on the Opalinus Clay samples, while in neighbouring boreholes of the same study area, samples were selected from the over- and underlying rock sequences. As the variation in diffusion parameters is linked to rock composition, the mineralogical profiles (derived from a multi-min dataset) representing the downhole rock variability (see Mazurek et al., 2023) are also presented. Since the uncharged HTO has minimal to no interactions with solid surfaces (Van Loon et al., 2003), its diffusion behaviour is considered as the reference case, primarily influenced by the pore structure. In the three study areas (Fig. 1), the diffusion coefficients of HTO are lowest in the Opalinus Clay and in few other samples in both the overlying and underlying units that are rich in clay or carbonate (Fig. 3).

On the other hand, the diffusion behaviour of charged species, unlike neutral species like HTO, is significantly influenced by both the pore structure and physico-chemical factors. For example, anions such as $^{36}Cl^-$ are repelled by negatively charged clay surfaces, the phenomenon known as anion exclusion. Consequently, their effective diffusion coefficient is lower compared to neutral species (as shown in Fig. 3), which is similar to the characteristic lower accessible porosity observed in previous studies (Appelo et al., 2010, Wigger and Van Loon, 2017) and discussed further in recent publications (Glaus et al., 2023; Zwahlen et al., 2023). The composition of the pore water has a significant effect on anion exclusion. When – as an example - comparing the results of OPA/BOZ1-1 (pore water with ionic strength of 0.19 M) with those of OPA/TRU1-1 (pore water with ionic strength of 0.35) and OPA/BUL1-1 (pore water with ionic strength of 0.505), it can be seen that $^{36}Cl^-$ diffuses on average 9.1 ± 1.4 times slower than HTO in the case of BOZ1-1, 5.6 ± 1.4 times slower in the case of TRU1-1 and only 4.61 ± 0.5 times slower in the case of BUL1-1.

Conversely, cations such as $^{22}Na^+$ preferentially interact with negatively charged clay surfaces, resulting in their enrichment in the solid/liquid boundary zone. As indicated in Fig. 3, the effective diffusion coefficient of $^{22}Na^+$ is, when normalized with the respective diffusion coefficients in bulk water, larger than that of HTO (and $^{36}Cl^-$), due to the contribution of adsorbed cations to the overall diffusive flux. This process is known as surface diffusion or surface-enhanced diffusion and has been extensively investigated in the past (Glaus et al., 2007; Appelo et al., 2010). Further details are found in Gimmi and Kosakowski (2011), Krejci et al. (2021) and Glaus et al. (2023). The composition of the porewater has an opposite effect on the diffusion parameters of $^{22}Na^+$ compared to $^{36}Cl^-$. In the case of OPA/BOZ1-1, diffusion of $^{22}Na^+$ is – after normalisation for the diffusion coefficients in water – on average 2.0 ± 0.8 times faster than HTO whereas in the case of OPA/TRU1-1 and OPA/BUL1-1 the diffusion is only 1.7 ± 0.4 and 1.9 ± 0.1 times faster, respectively.

The diffusion behaviour of $^{36}Cl^-$ seems to be more sensitive on ionic strength than that of $^{22}Na^+$. A more detailed discussion on effects of pore water composition on anion exclusion and surface diffusion is given in Glaus et al. (2023).

Fig. 4 presents box plots that summarize the measured effective diffusion coefficients and accessible porosity values (or R_d in the case of $^{22}Na^+$) for the study areas. The results shown in Fig. 4reveal that the effective diffusion coefficients for HTO and $^{22}Na^+$ in the Opalinus Clay across all three study areas are similar, approximately 1×10^{-11} m^2 s^{-1}, as is the effective diffusion coefficient of $^{36}Cl^-$ (approximately 1×10^{-12} m^2 s^{-1}). Furthermore, the distribution of the D_e values for the three tracers in the Opalinus Clay is relatively narrow, indicating that

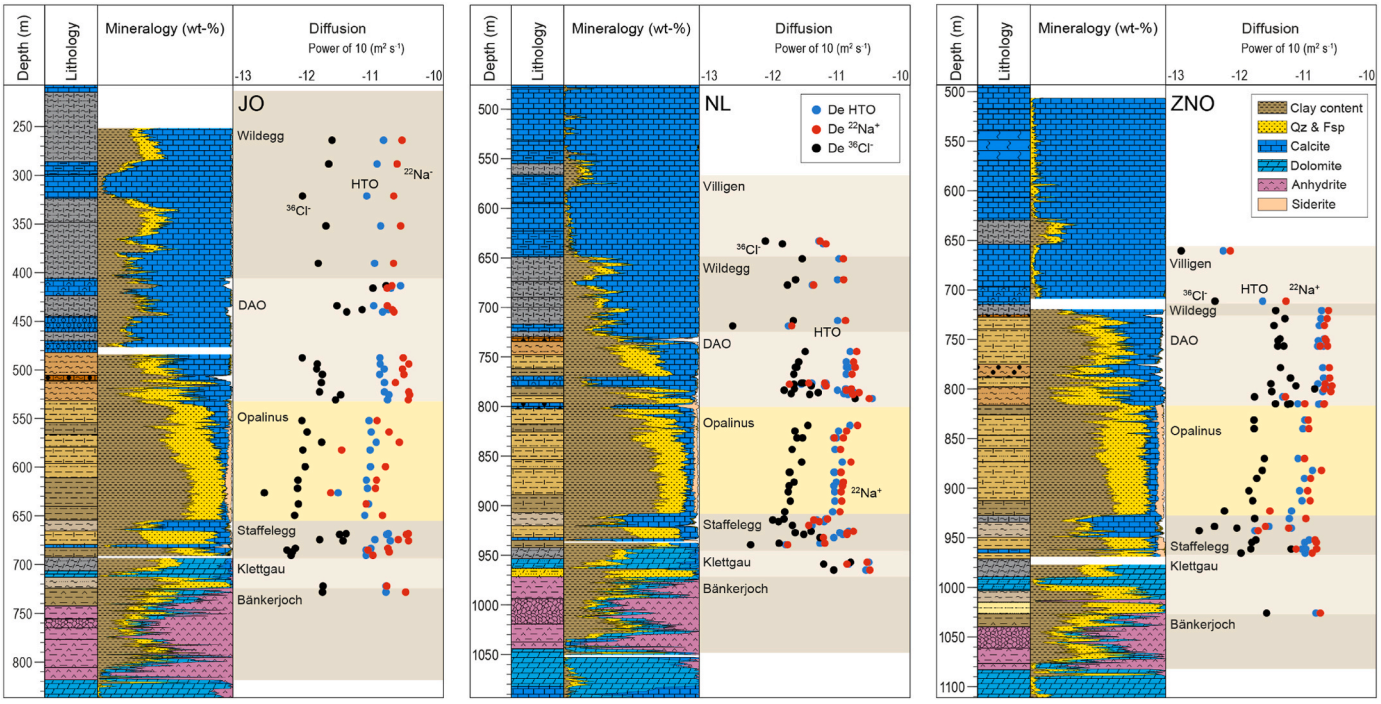

Fig. 3. Comparison of the effective diffusion coefficients of HTO, $^{36}Cl^-$ and $^{22}Na^+$ for Opalinus Clay (OPA), the Dogger above Opalinus Clay (DAO) and Malm, as well as the underlying Lias, Keuper and Triassic sediments for each study area (JO, NL, ZNO). Lithological units (see Mazurek et al., 2023 for detailed lithological data) and mineralogical compositions (dominant mineral phases only) based on a multi-min log approach (calibrated using core data) are also provided to illustrate the main compositional changes as a function of depth.

this layer has highly homogeneous diffusion properties. The accessible porosity values for HTO in Opalinus Clay have a value of approximately 0.12 and those for $^{36}Cl^-$ approximately 0.06. In contrast, the units above (Dogger, Malm) and below (Lias, Keuper, Trias) the Opalinus Clay exhibit greater variability in diffusion properties, indicating a more heterogeneous composition (Fig. 4). This heterogeneity observed in the rock units above and below the Opalinus Clay can be attributed to diverse sedimentary facies, varying deposition rates, and different diagenetic overprints. Consequently, these units have a more heterogeneous mineralogical composition, porosity and pore-space architecture. Nevertheless, the diffusion parameters of these rock units are still within the same order of magnitude as those observed in the Opalinus Clay.

This study investigated in detail the diffusive behaviour of different radiotracers in 130 sedimentary rock samples from the Opalinus Clay and the overlying Dogger and Malm as well as the underlying Lias, Keuper and Triassic units (between the bounding aquifers). The results show that the diffusion parameters of the Opalinus Clay are relatively consistent within each borehole and across the different study areas.

A comparison was also made between previous and current diffusion data of Opalinus Clay, with a specific focus on the diffusion coefficients of HTO. This analysis involved examining data from multiple boreholes and the Mont Terri Underground Rock Laboratory (https://www.mont-terri.ch/en/home.html). The results show a significantly narrow range of values (Fig. 5), ranging from 5×10^{-12} m^2 s^{-1} to 1.5×10^{-11} m^2 s^{-1}.

The samples from the Underground Rock Laboratory (URL) in Mont Terri (MT) (Fig. 1) have the highest values (Fig. 5), which may be due to lower maximum burial depth and thus higher total porosity compared to the rocks from the three study areas (Mazurek et al., 2006). Furthermore, the data shows that the samples from the study areas JO (BUL1-1), NL (TRU1-1), ZNO (Benken, TRU1-1) and borehole Schlattingen-1 (Fig. 1), yield similar values within a factor of two and there is no discernible impact of the current sample depth on the values of the effective diffusion coefficients.

4. Discussion

Archie's relationship and extensions of it were often used in previous studies (Bestel et al., 2018; Glaus et al., 2010; Van Loon and Mibus, 2015) for a simplistic empiric description of the effective diffusivity as a function of the total porosity of the porous medium.

In the present study, it is rather obvious that this approach will not provide a sufficient accuracy with the majority of the porosity values of the rock samples clustering around a value of ~0.1 and a rather large variability of the D_e values for HTO. Hence, the best-fit parameter values for the extended Archie's relationship provided in Van Loon and Mibus (2015) does not produce a valuable consistency with the results obtained for carbonate-rich rock samples (Fig. 6). For this reason, alternative empiric model descriptions are proposed here.

Because the presence of clay minerals determines several rock properties important for radionuclides migration processes (e.g., specific surface area, pore size distribution, cation exchange capacity), the correlation between diffusion parameters and total clay content is explored in the following. The diffusion of HTO is used to explore this correlation, as it is a neutral species that is not significantly affected by the chemical composition of the pore water. The effective diffusion coefficient, D_e, is defined by Ficks's first law as:

$$J = -D_e \frac{dC}{dx} \quad (5)$$

Where J represents the diffusive flux (mol m^{-2} s^{-1}), dC/dx represents the concentration gradient (mol m^{-4}) and D_e is the effective diffusion coefficient (m^2 s^{-1}). The relationship between the effective diffusion coefficient and the diffusion coefficient in bulk water (D_w) can be expressed as:

$$D_e = \frac{\delta \cdot \varepsilon}{\tau^2} \cdot D_w \quad (6)$$

Where ε is the total (accessible) porosity, δ is the constrictivity ac-

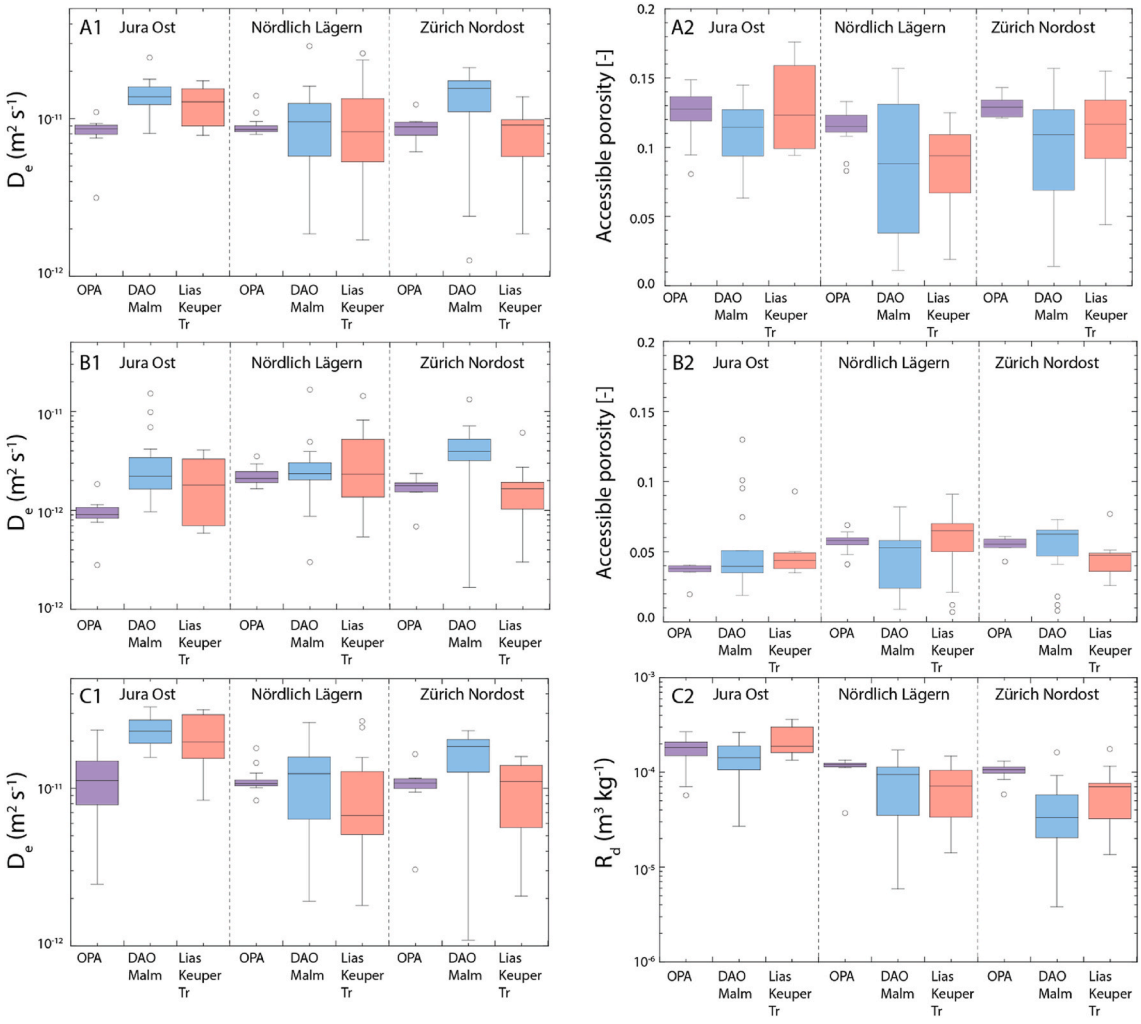

Fig. 4. Comparison of effective diffusion coefficients (A1, B1, C1) and accessible porosities of HTO (A2) and $^{36}Cl^-$ (B2), and R_d values for $^{22}Na^+$ (C2) for Opalinus Clay (OPA), and the samples from the overlying Dogger above Opalinus Clay (DAO) and Malm, as well as the underlying Lias, Keuper and Triassic sediments for each study area (JO, NL, ZNO). The boxes represent the median (line inside the box), and data within the first and third quartiles (upper and lower end of box). The whiskers indicate the variability outside the upper and lower quartiles (i.e. max and min values).

counting for the fact that the pore diameter varies along the diffusion pathway, and τ represents the tortuosity taking account for path lengthening (van Brakel and Heertjes, 1974). Because constrictivity and tortuosity cannot be determined independently, they are combined in the so-called geometrical factor G:

$$G = \frac{\tau^2}{\delta} \tag{7}$$

Equation (6) takes the form:

$$D_e = \frac{\varepsilon}{G} \cdot D_w \tag{8}$$

Equation (8) is used as the basis to test the parameter dependence on the total clay content. Fig. 7A displays the correlation between clay content and HTO-porosity (derived from diffusion of HTO) indicating that porosity is mainly associated with the clay phase of the rock, consistent with the findings of Mazurek et al. (2023). Fig. 7B shows the respective correlation of the geometrical factor which was calculated upon rearrangement of equation (8) from the best-fit parameter values for D_e and ε of HTO.

$$G = \frac{\varepsilon}{D_e} \cdot D_w \tag{9}$$

The value for D_w was taken from Li and Gregory (1974) and Woolf (1975) and has a value of 2.2×10^{-9} $m^2 s^{-1}$ at 25 °C. Molecular diffusion coefficients in the confined water of narrow clay pores tend to be smaller than bulk diffusion coefficients in free water (González Sánchez et al., 2008). This effect, however, depends on the size of the pores and the type of clay material. Because these properties are basically unknown and may differ among the various rock types investigated here, we assume for simplicity that bulk diffusion coefficients are applicable for clay pores.

In agreement with the box plots shown in Fig. 4, there is no discernible trend with respect to the study areas in the data shown in Fig. 7A and B.

The correlation between clay content and total porosity can be modelled by an empirical exponential function:

$$\varepsilon = m_1 * \left(1 - e^{-m_2 \cdot W_c}\right) \tag{10}$$

Where m_1 and m_2 are fitting constants and W_c represents the total clay content in weight percent (wt.%). The parameter m_1 represents a maximum total porosity value (ε_{max}) in the clay phase. A maximum total porosity of ca. 0.15 is observed at high clay content. The solid black line represents the best fit whereas the upper and lower curves represent upper and lower bounds at 3 sigma. The values of the parameters to calculate these curves are given in Table 2.

Mazurek et al. (2023) observed a similar dependency between the

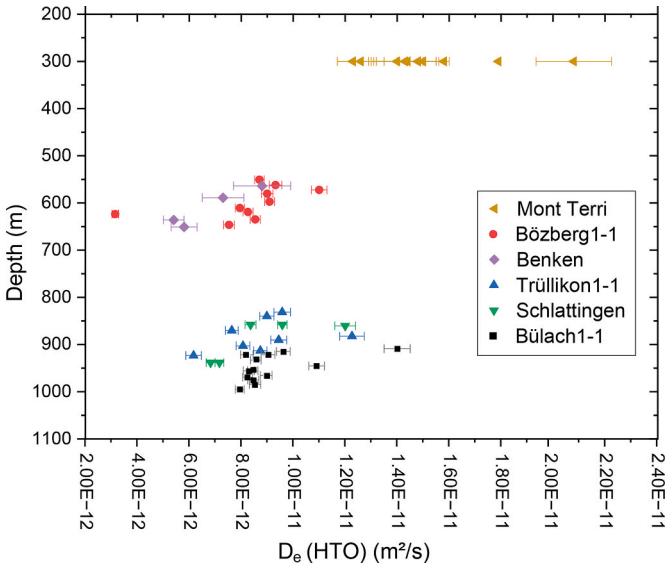

Fig. 5. Overview of the effective diffusion coefficients (perpendicular to the bedding plane) of HTO in OPA as a function of depth for samples from different boreholes and regions. Data for OPA-Mont Terri are taken from Van Loon et al. (2003), Van Loon et al. (2005), Joseph et al. (2013) and Wu et al. (2009). Data of Benken (Fig. 1) are taken from Van Loon et al. (2018) and those of Schlattingen-1 from Jacops et al. (2017) and Van Loon (2014).

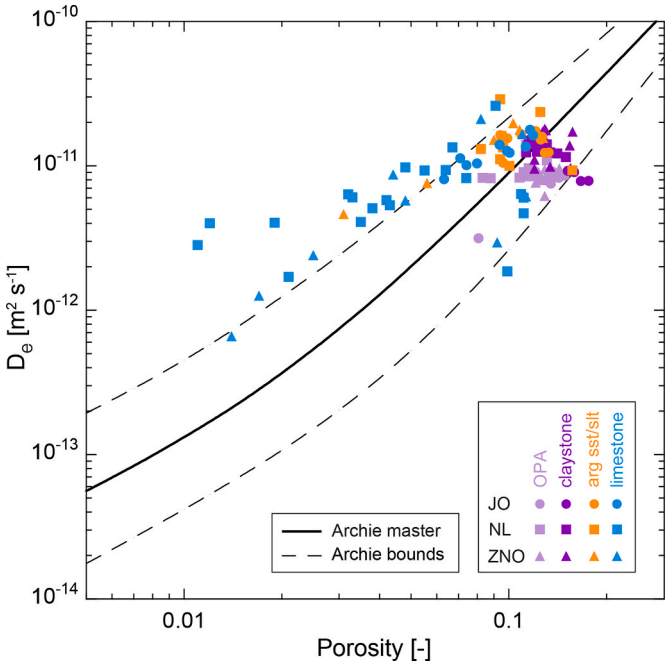

Fig. 6. Relationship between accessible porosity and effective diffusion coefficient of HTO (Archie's plot). The lines were calculated using the e-Archie equation and parameters given in Van Loon and Mibus (2015).

total clay content and the water-content porosity and observed a quasi-linear increase of the porosity at low clay content and a flattening of the curve for higher clay contents. They used a power-law function to fit the experimental data. The reason for the flattening of the curve will be explained later.

The geometrical factor significantly rises with increasing clay content beyond a clay content larger than approximately 30 wt%. Below this threshold, G remains relatively constant at a value of approximately 11 ± 4. According to the conceptual shale and microstructure model of Bourg and Ajo-Franklin (2017), shown in Fig. 8, the threshold value should be at $W_c = 34 \pm 10\%$, which supports the selected threshold of 30 wt% in this work. The outliers observed for limestones might be correlated with a large textural heterogeneity observed for these rock types and bi- or multi-modal pore size distributions (Mazurek et al., 2023). Empirical analysis of the data suggests a correlation between the geometrical factor and the total clay content that can be described by an empirical exponential function:

$$G = a_1 + e^{a_2 \cdot W_c} \quad (11)$$

Where a_2 is a fitting parameter and W_c represents the total clay content in weigh percent (wt.%). The value of a_1 was arbitrarily fixed at 10. The solid black line represents the best fit whereas the upper and lower curves represent upper and lower bounds at 3 sigma. The values of the parameters to calculate these curves are given in Table 3.

Argillaceous rocks are composed of a range of mineral grains of varying sizes (see also Mazurek et al., 2023), with clay minerals, apart from kaolinite, mainly falling in the range of 10 nm–20 μm or larger (chlorite, mica, kaolinite), and non-clay minerals such as quartz, carbonates and feldspars commonly in the order of 5 μm to greater than several millimetres. The size, grain fabric and grain texture (including diagenetic cements or recrystallized grains) and thus pore size and space depend on both depositional environment, source material as well as burial depth and diagenetic overprint, which can significantly alter the fabric and composition of the rocks (Wüst et al., 2018). The diffusive behaviour of solutes in sedimentary rocks often shows a strong dependency on the rock composition, with the clay phases playing a significant role, due to their large surface area and surface charge. Hence, clay-non-clay mineral aggregates, sizes, grain arrangement, intergranular pore space or pore connectivity are parameters determined by the rock type and diagenetic overprint (Mazurek et al., 2023). Thereby, in simplistic terms, the load-bearing phase in clay rocks depends on the composition with either the clay phase or the non-clay phase forming the load-bearing phase. This has significant implications for the rock's properties, including permeability, diffusivity (Dabat et al., 2019, 2020), mechanical strength (Bourg, 2015), and anisotropy of these properties.

In clay-rich rocks, the clay minerals are preferentially oriented perpendicular to the direction of sedimentation, whereas for clay-poor rocks the orientation is more random and depends on mineral sizes and aggregate fabric. According to Bourg (2015) and Bourg and Ajo-Franklin (2017), the critical clay content (W_c) where the change of preferential clay and clay mineral orientation occurs is approximately 34 wt% (weight fraction of clay $f_{clay} \approx 0.34$). Considering diffusion properties perpendicular to the bedding plane, it can be expected that the geometrical factor is larger in the case of clay-rich rocks (clay content >30 wt%) because of the larger tortuous diffusion pathways (τ is larger in equation (6)). In the case of clay-poor rocks (clay content ≤30 wt%), the geometrical factor is lower because of the more random orientation of the clay platelets between the grains (shelter effect of the larger grains during compaction of the sediments; see also Mazurek et al., 2023) resulting in a smaller tortuosity (making τ in equation (6) smaller). Conversely, in clay poor rocks, (clay content ≤30 wt%, $f_{clay} \leq 0.3$), the non-clay minerals form the load-bearing phase (Fig. 8) and limited compaction effect on the clay mineral orientation results in a relative constant G-value.

For clay contents ≥30 wt% ($f_{clay} \geq 0.3$) the clay minerals form the load-bearing phase (Fig. 8). The larger the clay content, the more pronounced the preferential orientation of the clay platelets, and the larger the G-value (Fig. 7). Evidence for such a behaviour is given in a previous study by Lash and Blood (2004). The authors investigated the orientation of clay platelets in black shale of the Upper Devonian (Frasnian) Rhinestreet shale of western New York State with ellipsoidal carbonate concretions. These concretions changed the elastic stress field in such a way that the sediments in the immediate near-field at the lateral edges of

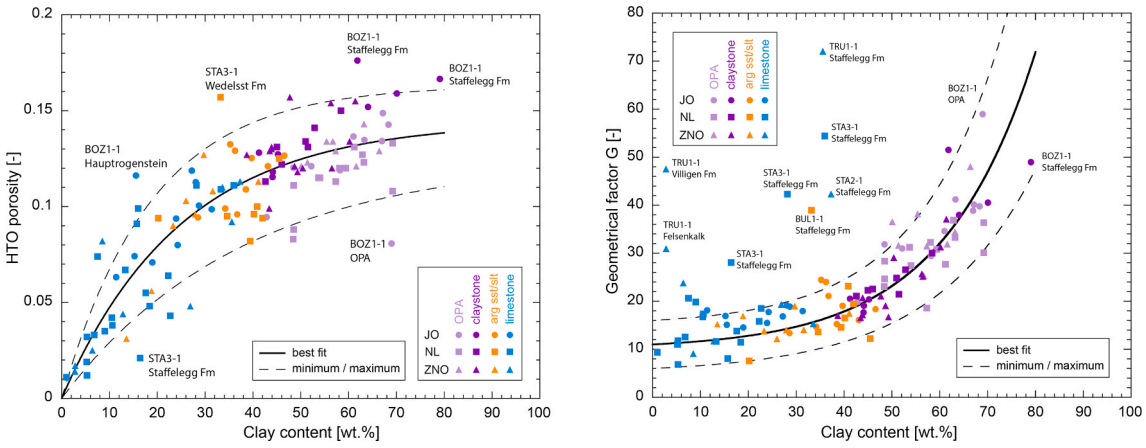

Fig. 7. A: Correlation between the HTO-porosity derived from diffusion of HTO and the clay content (wt.%). B: Correlation between the geometrical factor of HTO and the clay content of a sample (wt.%).

Table 2
Values of the parameters m_1 and m_2 used in Equation (10) to calculate the curves given in Fig. 7A.

parameter	Best value	1σ	3σ
m_1	0.1444	0.0063	0.0188
m_2	0.0398	0.0045	0.0134

the concretions were actually shielded from the overburden pressure by the creation of a so-called pressure shadow. This resulted in a merely random distribution of the clay platelets or in a house-of-cards fabric. Several tens of cm distant of the pressure shadows, the sediment was fully affected by the overburden stress leading to a preferential orientation of the clay or a strongly oriented microfabric (Lash and Blood, 2004).

It is important to point out that not only does the orientation of the clay platelets differ, but the porosity and bulk dry density of the clay phase might also change with clay content as well as progressive burial which increases clay crystallinity. If we assume that porosity within these diffusion-driven tight rocks of different origin within the Mesozoic sequence is associated with the clay phase, this porosity can be estimated from the weight fraction of clay minerals. The pore volume of the total rock ($V_{p,T}$) equals the pore volume of the clay phase ($V_{p,c}$):

$$V_{p,T} = V_{p,c} \tag{12}$$

The pore volume can be calculated from the porosity and the volume of the rock and/or minerals:

$$\varepsilon \cdot V_T = \varepsilon_c \cdot V_c \tag{13}$$

Where ε is the total porosity of the rock, ε_c is the porosity of the clay phase, V_T and V_c are the volumes of the total rock and the clay phase, respectively.

Equation (13) can be written as:

$$\varepsilon \cdot \frac{m_r}{\rho_{br}} = \varepsilon_c \cdot \frac{m_c}{\rho_{bc}} \tag{14}$$

where m_r and m_c are the masses of the rock and the clay phase, respectively, and ρ_{br} and ρ_{bc} represent the bulk dry densities of the rock and the clay phase. Rearranging equation (14) results in:

$$\varepsilon = \varepsilon_c \cdot \frac{m_c}{m_r} \cdot \frac{\rho_{br}}{\rho_{bc}} \tag{15}$$

with $f_{clay} = m_c/m_r$ (weight fraction of the clay phase)

$$\varepsilon = \varepsilon_c \cdot f_{clay} \cdot \frac{\rho_{br}}{\rho_{bc}} \tag{16}$$

The porosity of the clay phase can be written as:

$$\varepsilon_c = 1 - \frac{\rho_{bc}}{\rho_{gc}} \tag{17}$$

where ρ_{gc} is the grain density of the clay phase. Replacing ε_c in Equation (16) by Equation (17) gives:

$$\varepsilon = \left(1 - \frac{\rho_{bc}}{\rho_{gc}}\right) \cdot f_{clay} \cdot \frac{\rho_{br}}{\rho_{bc}} \tag{18}$$

Or after rearranging:

$$\varepsilon = f_{clay} \cdot \rho_{br} \cdot \left(\frac{1}{\rho_{bc}} - \frac{1}{\rho_{gc}}\right) \tag{19}$$

The porosity of the rock can be calculated from the weight fraction of the clay, the total bulk dry density of the rock, and the bulk dry density and the grain density of the clay phase.

The weight fraction of the clay is a variable and will change from 0.05 to 0.8. An average value of the bulk dry density of the rock was taken to be 2600 kg m^{-3}. This is not fully correct because the bulk dry density of the rock varies with the clay content. At low clay contents ρ_{br} ≈ 2700 kg m^{-3} whereas at high clay contents ρ_{b_r} ≈ 2500 kg m^{-3}. For the grain density of the clay phase a value of 2750 kg m^{-3} was selected.

Two scenarios were considered for the bulk dry density of the clay phase. In the first scenario (Fig. 9), a constant value of ρ_{bc} = 1900 kg m^{-3} was assumed, regardless of the clay content.

Such a scenario would result in a linear increase of the calculated porosity as a function of the clay content (shown by the blue curve in Fig. 9), which is in disagreement with the data shown in Fig. 5. However, the results in Fig. 9 show that for clay contents up to approximately 20–25 wt%, the calculated and measured porosity values are in good agreement when a constant ρ_{bc} is used. The choice of ρ_{bc} = 1900 kg m^{-3} is based on a trial-and-error approach giving the best results, at least for the lower clay content. For clay contents >25 wt%, the porosity is clearly overestimated when using ρ_{bc} = 1900 kg m^{-3}, suggesting that the assumed value is too low. In a second scenario (Fig. 9), the bulk dry density of the clay phase was kept constant until a clay content of approximately 25 wt% and was continuously increased (linearly) for clay contents >25 wt between ρ_{bc} = 2000 kg m^{-3} and ρ_{bc} = 2340 kg m^{-3}. The use of a variable bulk dry density resulted in a good agreement between the calculated porosity of the rocks and the data in Fig. 5. This indicates that the porosity of clay rocks is strongly influenced by the clay content (i.e. clay content dependent) and the magnitude of the load the

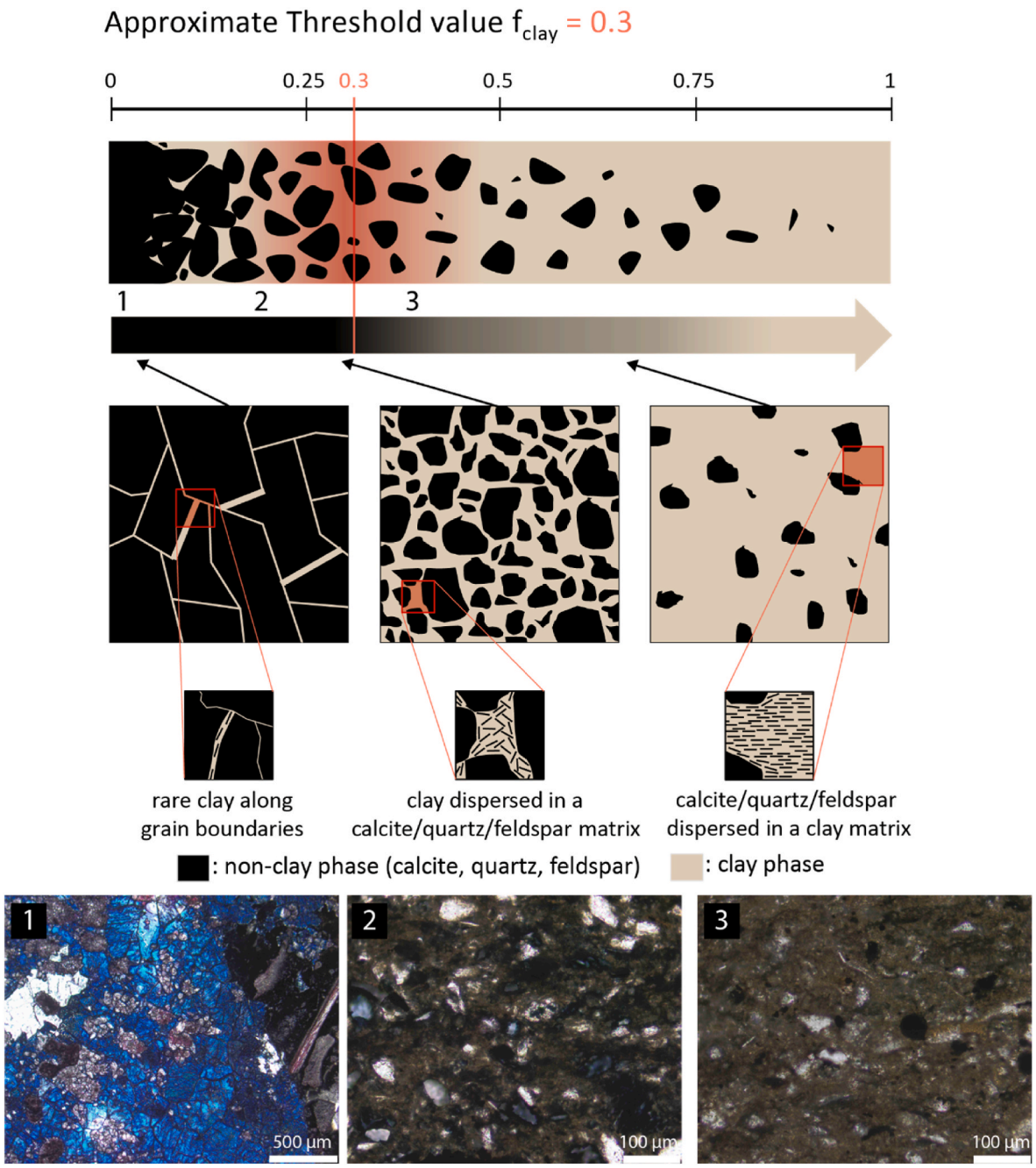

Fig. 8. Conceptual model of clay rocks with different amounts of fine-grained clay and coarse-grained calcite, quartz and feldspar. Figure (top) modified from Crawford et al. (2008), Houben et al. (2014), and Bourg (2015). Thin section images (bottom from left to right) display recrystallized carbonates, and silt- and claystones (all DAO).

Table 3
Values of the parameters a_0 and a_1 used in equation (11) to calculate the curves given in Fig. 7B.

parameter	Best value	1σ	3σ
a_1	10.0	2.0	6.0
a_2	0.0515	0.0016	0.0047

rock endured, or in simpler terms, the load-bearing characteristics of the clay phase.

Because there is no experimental way to determine ρ_{bc} in a rock sample, it is difficult to judge whether there is a continuous change of the dry density with clay content ($\rho_{bc} = f(W_c)$) or whether ρ_{bc} is constant to a given threshold value of clay content, e.g. 25 wt%, and changes for clay contents larger than this threshold value. However, according to the observed porosity values, it seems that ρ_{bc} at low and high total clay content must be different, i.e. the value at low clay content is lower than at high clay content, leaving the exact dependency on the clay content unknown. The clay bulk dry density might also affect the pore size distribution. It is expected that at lower bulk dry densities, the pore sizes are larger than in the case of higher bulk dry densities. In that sense, it can be expected that the pore size in low clay rocks is larger than in the case of clay-rich rocks, because - as discussed earlier - the clay bulk dry density is lower. This is in agreement with the pore size distribution measurements given in Mazurek et al. (2023). Beside tortuosity, also the pore size might affect the geometrical factor. A larger pore size results in

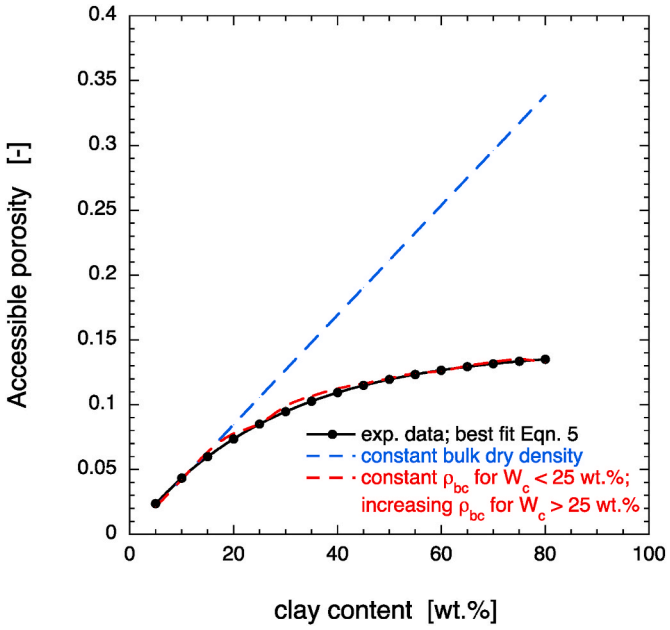

Fig. 9. Calculated and observed porosity values for samples with different mineral compositions. The blue line shows porosities calculated with Eqn. (18) using a clay bulk dry density of 1900 kg m^{-3}, irrespective of the clay content of the samples. The red curve shows porosities calculated with Eqn. (18) using ρ_{bc} = 1900 kg m^{-3} for a clay content <25 wt%, and an increasing ρ_{bc} for clay contents >25 wt%.

a larger pore constrictivity, δ, in Eqn. (7) and vice versa.

Combining equations (8), (10) and (11) results in an empirical equation that relates the effective diffusion coefficient to the total clay content:

$$D_e = \frac{m_1 \cdot (1 - e^{-m_2 \cdot W_c})}{a_1 + e^{a_2 \cdot W_c}} \cdot D_w \quad (20)$$

Fig. 10 visualises the correlation between the effective diffusion coefficient of HTO and the clay content of a sample. It can be seen that between a clay content of approximately 20 and 50 wt%, the dependency of the effective diffusion coefficient on the clay content is rather weak. Below a clay content of 20% and above a clay content of 50 wt%, the effective diffusion coefficient decreases with decreasing or increasing clay content.

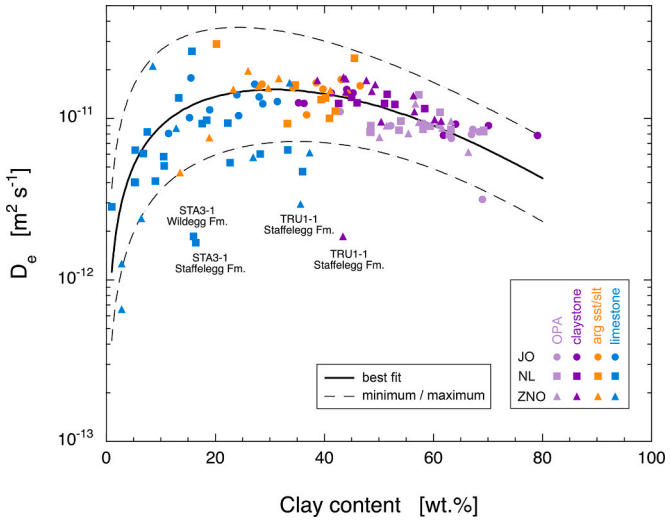

Fig. 10. Correlation between the effective diffusion coefficient of HTO and the total clay content of a sample. The solid line represents the best fit. Upper and lower curves represent the upper and lower bounds. Some of the outliers are labelled and are clay-rich samples with high amounts of organic carbon (4.7 and 7.8 wt%) from the Staffelegg Formation of borehole TRU1-1 (ZNO). Two other outliers are clay-poor samples with high calcite (79 and 74 wt%) but low organic carbon contents (0.36 and 0.28 wt%) and are from the Staffelegg and Wildegg Formation of the deep borehole STA3-1 (NL).

A model that includes more detailed information regarding mineralogical and textural properties, beyond what is presented in equation (20), would necessitate even more fundamental data. This is exemplified in Fig. 11, which shows a Füchtbauer diagramme (Füchtbauer, 1988), which is a graphical representation of the sedimentary rocks in terms of their clay minerals, carbonates, and quartz-feldspar assemblages. Within the ternary diagramme, sample distribution is displayed together with diffusion parameter values, such as G, porosity and D_e for HTO. The diagram reveals several distinct trends regarding the correlations of mineralogy and diffusion parameters.

The Füchtbauer diagramme (Fig. 11) shows that an increase in clay minerals leads to a rise in both the geometrical factor and porosity (as well as external surface area), regardless of the presence of calcite and quartz. The geometrical factor increases from approximately 10 in the

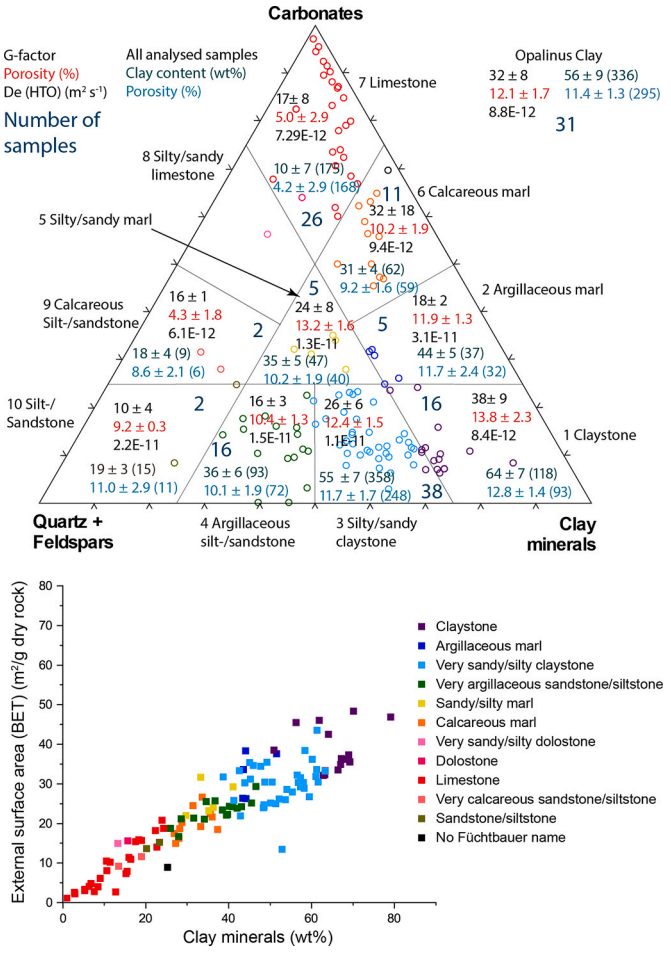

Fig. 11. Füchtbauer diagramme (top) illustrating diffusion parameters within the ternary diagramme of carbonates (calcite, dolomite, ankerite), quartz and feldspars (K-feldspar, plagioclase), and clay minerals (illite, smectite, kaolinite, chlorite) as end members. These parameters include geometrical factor, accessible porosity and effective diffusion coefficient of HTO. The diagramme demonstrates that G-factor and porosity generally increase from both quartz and feldspars and carbonate end-members towards the clay mineral end-member. Conversely, D_e, the effective diffusion coefficient of HTO, is lowest in limestones. The relationship between BET and total clay content (bottom) illustrates that high carbonate content samples within these Mesozoic sequences in Switzerland have low BET and also low diffusion coefficients.

siltstone/sandstones to 38 in the claystones, while the carbonate line shows a value of 17 for limestones, 32 for calcareous marls, and 18 for argillaceous marls. These findings align with those presented in Fig. 7. The impact of quartz and calcite on pore microstructure differs depending on the clay content, with an increase in quartz content resulting in a decrease in the geometrical factor but an increase in porosity when clay content is below 30–40 wt% (Fig. 7). The concurrent trends of porosity and geometry factors from carbonates and quartz/feldspars, respectively, to clay minerals partially offset each other in terms of the structure of equation (8) and the individual parameter dependencies. As a result, porosity and the geometrical factor are more informative and useful for a detailed and far-reaching description of the data in general.

These observed trends (Fig. 11) suggest that in addition to mineralogy, diagenesis may have a significant influence on pore microstructure (see also Mazurek et al., 2023). Quartz and carbonate minerals differ primarily in terms of their grain-size distribution, with carbonates having a broader range including recrystallized microfossils as well as having a greater likelihood of pressure solution or matrix cementation (i.e. micrite, sparite) (see also Wüst et al., 2018). However, without relevant data and supporting arguments, such hypotheses remain speculative.

To investigate the impact of mineral composition, diagenesis, and pore structure on diffusion in sedimentary rocks, further petrographic or microscopic (including scanning electron microscopy, see Bollermann et al., 2022) studies are necessary. These studies should focus on rock samples with higher quartz content, such as silt/sandstone and calcareous silt/silty sandstone samples and provide additional structural information.

The effective diffusion coefficient (D_e) of HTO exhibits minimal variation along the line of the clay-carbonate end members but rises from clay towards the quartz endmember. However, this trend is based on varying sample numbers within the different categories and therefore only has limited statistical significance.

5. Conclusions

This study investigated the diffusion properties of HTO, $^{36}Cl^-$ and $^{22}Na^+$ in samples with varying mineral composition collected from deep boreholes in the Mesozoic sediment sequence of northern Switzerland. Through-diffusion experiments were conducted to calculate effective diffusion coefficients and diffusion accessible porosities. The results showed that Opalinus Clay is quite homogenous in terms of effective diffusion coefficients and accessible porosities, with porosities of the neutral species HTO similar within a factor of two ($D_e = 8.8 \pm 1.9 \times 10^{-12}$ m^2 s^{-1}; $\varepsilon = 0.12 \pm 0.02$). In contrast, the diffusion properties of the diffusive-driven over- and underlying rock units, between the Malm and Keuper/Triassic aquifers, exhibit a wider range, which reflects the more heterogenous nature of sedimentary origin, deposition and diagenetic overprints. The effective diffusion coefficients and accessible porosities of HTO do not depend on the chemical composition of the pore water.

Anion exclusion effects led to generally smaller diffusion coefficients and accessible porosities of anions like $^{36}Cl^-$. Cations such as $^{22}Na^+$ showed larger diffusion coefficients due to surface enhanced diffusion. The extent of anion exclusion and surface diffusion effects depends on the composition of the pore water, and in the case of cations, the extent of sorption, which depends on the sorption capacity of the solid. As a result, differences in the effective diffusion coefficient of $^{36}Cl^-$ and $^{22}Na^+$ between different areas can be observed due to the different chemical composition of the pore waters in contact with the solid phase. Comparison of the results for OPA from BOZ1-1 (where the pore water has the lowest ionic strength), TRU1-1 (where the pore water has an intermediate ionic strength) and BUL1-1 (where the pore water has the highest ionic strength) reveals that $^{36}Cl^-$ diffuses, on average, 9.1 ± 1.4 times slower than HTO in the case of BOZ1-1, and 5.6 ± 1.4 in the case of TRU1-1, while in the case of BUL1-1, it only diffuses 4.1 ± 0.5 times slower. When the diffusion coefficients in water are normalized, the diffusion of $^{22}Na^+$ is, on average, 2.0 ± 0.8 times faster than HTO in BOZ1-1 and 1.9 ± 0.1 and 1.7 ± 0.4 times faster in BUL1-1 and TRU1-1, respectively. Anion diffusion is more sensitive on changes in pore water composition than cation diffusion.

A correlation was also observed between the diffusion coefficients and the total clay content of the samples. The results suggest the possibility of developing procedures for calculating generalised diffusion coefficients for units with varying clay content. However, in samples with low clay content, the model and derivation and its dependency will require further investigations.

Declaration of competing interest

The authors declare that they have no known competing financial interests or personal relationships that could have appeared to influence the work reported in this paper.

Data availability

Data are given in the attached Supporting Information file (SI)

Acknowledgement

The authors express their gratitude to several individuals and institutions for their assistance in the research project. Specifically, they thank the members of the RWI (University of Bern), including M. Mazurek, T. Gimmi, and C. Zwahlen, as well as members of Nagra, in particular D. Traber and J. Becker, for their contributions in sample selection, evaluation and support with auxiliary data. The technical illustration office and Fabian Maier at Nagra are also acknowledged for their efforts in finalizing the figures. Marc Aertsens (SCK-CEN) is thanked for valuable input to the manuscript and Sven Friedel (Comsol Multiphysics) for help with numerical simulations. The authors extend special thanks to Nagra (National Cooperative for the Disposal of Radioactive Waste, Wettingen, Switzerland) for providing financial support, which enabled the successful completion of this study.

Appendix A. Supplementary data

Supplementary data to this article can be found online at https://doi.org/10.1016/j.apgeochem.2023.105843.

References

Aertsens, M., Van Gompel, M., De Cannière, P., Maes, N., Dierckx, A., 2008. Vertical distribution of $H^{14}CO_3^-$ transport parameters in Boom clay in the Mol-1 borehole (Mol, Belgium). Phys. Chem. Earth 33, S61–S66.

Aldaba, D., Glaus, M., Leupin, O., Van Loon, L., Vidal, M., Rigol, A., 2014. Suitability of various materials for porous filters in diffusion experiments. Radiochim. Acta 102, 723–730.

Appelo, C.A.J., Wersin, P., 2007. Multicomponent diffusion modeling in clay systems with application to the diffusion of tritium, iodide, and sodium in Opalinus Clay. Environ. Sci. Technol. 41, 5002–5007.

Appelo, C.A.J., Van Loon, L.R., Wersin, P., 2010. Multicomponent diffusion of a suite of tracers (HTO, Cl, Br, I, Na, Sr, Cs) in a single sample of Opalinus Clay. Geochim. Cosmochim. Acta 74, 1201–1219.

Aschwanden, L., Camesi, L., Gimmi, T., Jenni, A., Kiczka, M., Mäder, U., Mazurek, M., Rufer, D., Waber, H.N., Wersin, P., Zwahlen, C., Traber, D., 2021. TBO Trüllikon-1-1: Data Report Dossier VIII Rock Properties, Porewater Characterisation and Natural Tracer Profiles. Report NAB 20-09. Nagra, Wettingen, Switzerland.

Bazer-Bachi, F., Tevissen, E., Descostes, M., Grenut, B., Meier, P., Simonnot, M.-O., Sardin, M., 2006. Characterization of iodide retention on Callovo-Oxfordian argillites and its influence on iodide migration. Phys. Chem. Earth 31, 517–522.

Bestel, M., Glaus, M.A., Frick, S., Gimmi, T., Juranyi, F., Van Loon, L.R., Diamond, L.W., 2018. Combined tracer through-diffusion of HTO and ^{22}Na through Na-montmorillonite with different bulk dry densities. Appl. Geochem. 93, 158–166.

Bollermann, T., Yuan, T., Kulenkampff, J., Stumpf, T., Fischer, C., 2022. Pore network and solute flux pattern analysis towards improved predictability of diffusive transport in argillaceous host rocks. Chem. Geol. 606, 120997.

Bossart, P., Thury, M., 2007. Research in the Mont Terri rock laboratory: quo vadis? Phys. Chem. Earth 32, 19–31.
Bourg, I., 2015. Sealing shales versus brittle shales: a sharp threshold in the material properties and energy technology uses of fine-grained sedimentary rocks. Environ. Sci. Technol. Lett. 2, 255–259.
Bourg, I.C., Ajo-Franklin, J.B., 2017. Clay, water, and salt: controls on the permeability of fine-grained sedimentary rocks. Acc. Chem. Res. 50, 2067–2074.
Cavé, L., Al, T., Xiang, Y., Vilks, P., 2009. A technique for estimating one-dimensional diffusion coefficients in low-permeability sedimentary rock using X-ray radiography: comparison with through-diffusion measurements. J. Contam. Hydrol. 103, 1–12.
Crawford, B.R., Faulkner, D.R., Rutter, E.H., 2008. Strength, porosity, and permeability development during hydrostatic and shear loading of synthetic quartz-clay fault gouge. J. Geophys. Res. 113, B3207.
Dabat, T., Porion, P., Hubert, F., Paineau, E., Dazas, B., Grégoire, B., Tertre, E., Delville, A., Ferrage, E., 2020. Influence of preferred orientation of clay particles on the diffusion of water in kaolinite porous media at constant porosity. Appl. Clay Sci. 184, 105354.
Dabat, T., Hubert, F., Paineau, E., Launois, P., Laforest, C., Grégoire, B., Dazas, B., Tertre, E., Delville, A., Ferrage, E., 2019. A general orientation distribution function for clay-rich media. Nat. Commun. 10, 1–9.
Descostes, M., Blin, V., Bazer-Bachi, F., Meier, P., Grenut, B., Radwan, J., Schlegel, M.L., Buschaert, S., Coelho, D., Tevissen, E., 2008. Diffusion of anionic species in Callovo-Oxfordian argillites and Oxfordian limestones (Meuse/Haute-Marne, France). Appl. Geochem. 23, 655–677.
Dutt, G.R., Low, P.F., 1962. Diffusion of alkali chlorides in clay–water systems. Soil Sci. 47, 233–240.
Füchtbauer, H., 1988. Sedimente und Sedimentgesteine. Sediment-Petrologie, Teil II. Schweizerbart Science Publisher, Stuttgart, Germany. ISBN 978-3-510-65138-2.
Gimmi, T., Leupin, O.X., Eikenberg, J., Glaus, M.A., Van Loon, L.R., Waber, N., et al., 2014. Anisotropic diffusion at the field scale in a 4-year multi-tracer diffusion and retention experiment - I: insights from the experimental data. Geochim. Cosmochim. Acta 125, 373–393.
Gimmi, T., Kosakowski, G., 2011. How mobile are sorbed cations in clays and clay rocks? Environ. Sci. Technol. 45, 1443–1449.
Gimmi, T., Waber, H.N., 2004. Modelling of Tracer Profiles in Pore Water of Argillaceous Rocks in the Benken Borehole: Stable Water Isotopes, Chloride, and Chlorine Isotopes. Technical Report NTB 04-05. Nagra, Wettingen, Switzerland.
Glaus, M.A., Frick, S., Rossé, R., Van Loon, L.R., 2010. Comparative study of tracer diffusion of HTO, $^{22}Na^{+}$ and $^{36}Cl^{-}$ in compacted kaolinite, illite and montmorillonite. Geochim. Cosmochim. Acta 74, 1999–2010.
Glaus, M.A., Frick, S., Van Loon, L.R., 2021. Competitive effects of cations on the diffusion properties of strongly sorbing trace cations in compacted illite and Opalinus Clay. Earth Space Chem 5, 2621–2625.
Glaus, M.A., Frick, S., Van Loon, L.R., 2020. A coherent approach for cation surface diffusion in clay minerals and cation sorption models: diffusion of Cs^{+} and Eu^{3+} in compacted illite as case examples. Geochim. Cosmochim. Acta 274, 79–96.
Glaus, M.A., Frick, S., Van Loon, L.R., 2017. Diffusion of Selected Cations and Anions in Compacted Montmorillonite and Bentonite. PSI Bericht 17-07. Paul Scherrer Institut, Villigen PSI, Switzerland.
Glaus, M.A., Aertsens, M., Appelo, C.A.J., Kupcik, T., Maes, N., Van Laer, L., Van Loon, L. R., 2015. Cation diffusion in the electrical double layer enhances the mass transfer rates for Sr^{2+}, Co^{2+} and Zn^{2+} in compacted illite. Geochim. Cosmochim. Acta 165, 376–388.
Glaus, M.A., Rossé, R., Van Loon, L.R., Yaroshchuk, A.E., 2008. Tracer diffusion in sintered stainless-steel filters: measurement of the effective diffusion coefficients and implications for diffusion studies with compacted clays. Clays Clay Miner. 56, 677, 2008.
Glaus, M.A., Baeyens, B., Bradbury, M.H., Jakob, A., Van Loon, L.R., Yaroshchuk, A., 2007. Diffusion of ^{22}Na and ^{85}Sr in Montmorillonite: evidence of interlayer diffusion being the dominant pathway at high compaction. Environ. Sci. Technol. 41, 478–485.
Glaus, M.A., Van Loon, L.R., Wüst, R.A.J., 2023. Diffusion of HTO, ^{36}Cl and ^{22}Na in the Mesozoic rocks of northern Switzerland. II: Data interpretation in terms of an electrical double layer model. Appl. Geochem., 105842. https://doi.org/10.1016/j.apgeochem.2023.105842.
González Sánchez, F., Jurányi, F., Gimmi, T., Van Loon, L., Unruh, T., Diamond, L.W., 2008. Translational diffusion of water and its dependence on temperature in charged and uncharged clays: a neutron scattering study. J. Chem. Phys. 129, 174706.
Houben, M.E., Desbois, G., Urai, J.L., 2014. A comparative study of representative 2D microstructures in Shaly and Sandy facies of Opalinus Clay (Mont Terri, Switzerland) inferred form BIB-SEM and MIP methods. Mar. Petrol. Geol. 49, 143–161.
Hummel, W., Thoenen, T., 2023. The PSI Chemical Thermodynamic Database 2020. Nagra Technical Report NTB 21-03. Nagra, Wettingen, Switzerland.
Jacops, E., Aertsens, M., Maes, N., Bruggeman, C., Swennen, R., Krooss, B., Amann-Hildenbrand, A., Littke, R., 2017. The dependency of diffusion coefficients and geometric factor on the size of the diffusing molecule: observations for different clay-Based materials. Geofluids 2017, 8652560.
Joseph, C., Van Loon, L.R., Jakob, A., Steudtner, R., Schmeide, K., Sachs, S., Bernhard, G., 2013. Diffusion of U(VI) in Opalinus clay: influence of temperature and humic acid. Geochim. Cosmochim. Acta 109, 74–89.
Kaplan, U., 2013. Speziation von Plutonium bei der Sorption und Diffusion in Opalinuston. PhD Thesis. JJohannes Gutenberg University, Mainz, Germany, 104 pp.
Krejci, P., Gimmi, T., Van Loon, L.R., 2021. On the concentration-dependent diffusion of sorbed cesium in Opalinus Clay. Geochim. Cosmochim. Acta 298, 149–166.
Lash, G.G., Blood, D.R., 2004. Origin of shale fabric by mechanical compaction of flocculated clay: evidence from the upper Devonian Rhinestreet Shale, Western New York, USA. J. Sediment. Res. 74, 110–116.
Leupin, O.X., Van Loon, L.R., Gimmi, T., Wersin, P., Soler, J.M., 2017. Exploring diffusion and sorption processes at the Mont Terri rock laboratory (Switzerland): lessons learned from 20 years of field research. Swiss J. Geosci. 110, 391–403.
Li, Y.-H., Gregory, S., 1974. Diffusion of ions in sea water and in deep-sea sediments. Geochim. Cosmochim. Acta 38, 703–714.
Lübke, M., 2015. Migration von Technetium in natürlichem Tongestein. PhD Thesis. Johannes Gutenberg University, Mainz, Germany, 187 pp.
Mazurek, M., Gimmi, T., Zwahlen, C., Aschwanden, L., Gaucher, E.C., Kiczka, M., Rufer, D., Wersin, P., Marques Fernandes, M., Glaus, M.A., Van Loon, L.R., Traber, D., Schnellmann, M., Vietor, T., 2023. Swiss deep drilling campaign 2019–2022: Geological overview and rock properties with focus on porosity and pore-space architecture. Appl. Geochem. 105839. https://doi.org/10.1016/j.apgeochem.2023.105839.
Mazurek, M., Aschwanden, L., Camesi, L., Gimmi, T., Jenni, A., Kiczka, M., Mäder, U., Rufer, D., Waber, H.N., Wanner, P., Wersin, P., Traber, D., 2021. TBO Bülach-1-1: Data Report Dossier VIII Rock Properties, Porewater Characterisation and Natural Tracer Profiles. Report NAB 20-08. Nagra, Wettingen, Switzerland.
Mazurek, M., Alt-Epping, P., Bath, A., Gimmi, T., Waber, H.N., Buschaert, S., De Cannière, P., De Craen, M., Gautschi, A., Savoye, S., Vinsot, A., Wemaere, I., Wouters, L., 2011. Natural tracer profiles across argillaceous formations. Appl. Geochem. 26, 1035–1064.
Mazurek, M., Hurford, A.J., Leu, W., 2006. Unravelling the multi-stage burial history of the Swiss Molasse Basin: integration of apatite fission track, vitrinite reflectance and biomarker isomerisation analysis. Basin Res. 18, 27–50.
Nagra, 2021. The Nagra Research, Development and Demonstration (RD&D) Plan for the Disposal of Radioactive Waste in Switzerland. Technical Report NTB 21-02. Nagra, Wettingen, Switzerland.
Nagra, 2002. Project Opalinus Clay: Safety Report - Demonstration of Disposal Feasibility for Spent Fuel, Vitrified High-Level Waste and Long-Lived Intermediate-Level Waste (Entsorgungsnachweis). Technical Report NTB 02-05. Nagra, Wettingen, Switzerland.
Nagra, 2001. Sondierbohrungen Benken: Untersuchungsbericht. Technical Report NTB 00-01. Nagra, Wettingen, Switzerland.
Savoye, S., Goutelard, F., Beaucaire, C., Charles, Y., Fayette, A., Herbette, M., Larabi, Y., Coelho, D., 2011. Effect of temperature on the containment properties of argillaceous rocks: the case study of Callovo-Oxfordian claystones. J. Contam. Hydrol. 125, 102–112.
van Brakel, J., Heertjes, P.M., 1974. Analysis of diffusion in macroporous media in terms of a porosity, a tortuosity and a constrictivity factor. Int. J. Heat Mass Tran. 17, 1093–1103.
Van Laer, L., Aertsens, M., Maes, N., Van Loon, L.R., Glaus, M.A., Wüst, R.A.J., 2023. Diffusion of HTO, ^{36}Cl and ^{22}Na in the Mesozoic rocks of northern Switzerland. III: Cross-lab comparison of diffusion measurements on argillaceous twin samples. Appl. Geochem., 105840. https://doi.org/10.1016/j.apgeochem.2023.105840.
Van Loon, L.R., Glaus, M.A., Wüst, R.A.J, 2023. Diffusion Measurements of HTO, $^{36}Cl^{-}$ and $^{22}Na^{+}$ on rock samples of Opalinus Clay and confining units from deep bore holes at the potential siting regions for a deep geological repository for radioactive waste in Switzerland: Jura Ost, Nördlich Lägern and Zürich Nordost. Report NAB 23-26. Nagra, Wettingen, Switzerland.
Van Loon, L.R., Leupin, O.X., Cloet, V., 2018. The diffusion of SO_4^{2-} in Opalinus Clay: measurements of effective diffusion coefficients and evaluation of their importance in view of microbial mediated reactions in the near field of radioactive waste. Appl. Geochem. 95, 19–24.
Van Loon, L.R., 2014. Effective Diffusion Coefficients and Porosity Values for Argillaceous Rocks and Bentonite: Measured and Estimated Values for the Provisional Safety Analyses for SGT-E2. Technical Report NTB 12-03. Nagra, Wettingen, Switzerland.
Van Loon, L.R., Mibus, J., 2015. A modified version of Archie's law to estimate effective diffusion coefficients of radionuclides in argillaceous rocks and its application in safety analysis studies. Appl. Geochem. 59, 85–94.
Van Loon, L.R., Baeyens, B., Bradbury, M.H., 2009. The sorption behaviour of caesium on Opalinus Clay: a comparison between intact and crushed material. Appl. Geochem. 24, 999–1004.
Van Loon, L.R., Müller, W., Iijima, K., 2005. Activation energies of the self-diffusion of HTO, $^{22}Na^{+}$ and $^{36}Cl^{-}$ in a highly compacted argillaceous rock (Opalinus Clay). Appl. Geochem. 20, 961–972.
Van Loon, L.R., Soler, J.M., Müller, W., Bradbury, M.H., 2004. Anisotropic diffusion in layered argillaceous rocks: a case study with Opalinus Clay. Environ. Sci. Technol. 38, 5721–5728.
Van Loon, L.R., Soler, J.M., 2003. Diffusion of HTO, $^{36}Cl^{-}$, $^{125}I^{-}$ and $^{22}Na^{+}$ in Opalinus Clay: Effect of Confining Pressure, Sample Orientation, Sample Depth and Temperature. Technical Report NTB 03-07. Nagra, Wettingen, Switzerland.
Van Loon, L.R., Soler, J.M., Jakob, A., Bradbury, M.H., 2003. Diffusion of HTO, $^{36}Cl^{-}$ and $^{125}I^{-}$ in Opalinus clay samples from Mont Terri: effect of confining pressure. J. Contam. Hydrol. 61, 73–83.
Wenk, H.-R., Voltolini, M., Mazurek, M., Van Loon, L.R., Vinsot, A., 2008. Preferred orientations and anisotropy in shales: Callovo-Oxfordian shale (France) and Opalinus Clay (Switzerland). Clay Clay Miner. 56, 285–306.
Wersin, P., Mazurek, M., Waber, H.N., Mäder Urs, K., Gimmi, T., Rufer, D., de Haller, A., 2013. Rock and Porewater Characterisation on Drillcores from the Schlattingen Borehole. Report NAB 12-54. Nagra, Wettingen, Switzerland.

Wersin, P., Gimmi, T., Mazurek, M., Alt-Epping, P., Pękala, M., Traber, D., 2018. Multicomponent diffusion in a 280 m thick argillaceous rock sequence. Appl. Geochem. 95, 110–123.

Wersin, P., Aschwanden, L., Camesi, L., Gaucher, E.C., Gimmi, T., Jenni, A., Kiczka, M., Mäder, U., Mazurek, M., Rufer, D., Waber, H.N., Zwahlen, C., Traber, D., 2022. TBO Bözberg-1-1: Data Report Dossier VIII Rock Properties, Porewater Characterisation and Natural Tracer Profiles. Report NAB 21-21. Nagra, Wettingen, Switzerland.

Wigger, C., Van Loon, L.R., 2017. Importance of interlayer equivalent pores for anion diffusion in clay-rich sedimentary rocks. Environ. Sci. Technol. 51, 1998–2006.

Woolf, L.A., 1975. Tracer diffusion of tritiated water (THO) in ordinary water (H_2O) under pressure. J. Chem. Soc., Faraday Trans. 1 (71), 784–796.

Wu, T., Amayri, S., Drebert, J., Van Loon, L.R., Reich, T., 2009. Neptunium(V) sorption and diffusion in Opalinus clay. Environ. Sci. Technol. 43, 6567–6571.

Wüst, R.A.J., Tu, S., Nassichuk, B., Bozarth, T., Tucker, J., Cui, A., 2018. Chemostratigraphy, petrography, and SEM investigations of the Lower Triassic Montney Formation in Alberta: implications for a new and revised diagenetic and depositional model. Bull. Can. Petrol. Geol. 66, 436–471.

Xiang, Y., Al, T., Mazurek, M., 2016. Effect of confining pressure on diffusion coefficients in clay-rich, low-permeability sedimentary rocks. J. Contam. Hydrol. 1–10.

Xiang, Y., Al, T., Scott, L., Loomer, D., 2013. Diffusive anisotropy in low-permeability Ordovician sedimentary rocks from the Michigan Basin in southwest Ontario. J. Contam. Hydrol. 155, 31–45.

Zwahlen, C., Gimmi, T., Jenni, A., Kiczka, M., Mazurek, M., Van Loon, L.R., Mäder, U., Traber, D., 2023. Chloride accessible porosity fractions across the Jurassic sedimentary rocks of northern Switzerland. Appl. Geochem, 105841. https://doi.org/10.1016/j.apgeochem.2023.105841.